A Probabilistic Model for Failure of Polycrystalline Silicon MEMS Structures

A THESIS
SUBMITTED TO THE FACULTY OF THE GRADUATE SCHOOL
OF THE UNIVERSITY OF MINNESOTA
BY

Zhiren Zhu

IN PARTIAL FULFILLMENT OF THE REQUIREMENTS
FOR THE DEGREE OF
MASTER OF SCIENCE

Roberto Ballarini **Jia-Liang Le**

May, 2015

Acknowledgements

I would like to express my sincere gratitude to my advisors, Dr. Roberto Ballarini and Dr. Jia-Liang Le, for their patient guidance during my time here at the University of Minnesota. Special thanks also go to my fellow graduate student, Bing Xue, who kindly offered help and suggestions for the construction of FE models used in this project. I would also like to acknowledge the support of the University of Minnesota Supercomputing Institute, without which I would be unable to complete such a high volume of computational simulations.

Abstract

Reliable MEMS devices are expected to have a very low failure probability, and thus it is cost-prohibitive to determine design strength values merely based on extensive histogram testings. A theoretical understanding of probabilistic failure in the structure is critical for reliability analysis of MEMS devices. Prediction of failure statistics for MEMS structures are commonly based on the classical Weibull's model for material strength, which has been experimentally proven to be incapable of optimally fitting the failure probability distribution of MEMS structures. A generalized finite weakest-link model is developed to describe the strength statistics of polycrystalline silicon (poly-Si) MEMS structures. Different from the classical Weibull statistics based on extreme value statistics, the present model is applicable for poly-Si structures of all sizes. The overall failure probability of the structure is related to the failure probability of each material element along its sidewalls through a weakest-link statistical model. For each material element, the failure statistics is determined by both the random material strength and stress field induced by random sidewall geometry. The model is shown to agree well with measured strength histograms of poly-Si MEMS specimens of different sizes, and the calibrated mean strength of the material element is in accordance with theoretical strength of silicon. The strength statistics is further related to the effects of structure size on the mean structural strength, and an efficient method to determine the failure statistics of MEMS structures is proposed based on the present model.

Contents

Acknowledgements **i**

Abstract **ii**

List of Tables **v**

List of Figures **vi**

1 Introduction **1**

2 Weibull's Weakest Link Model for Material Strength **5**

2.1 Formulation of Weibull's model 5

2.2 Weibull distribution in extreme value statistics 7

2.3 Prediction of nominal strength using Weibull model 11

2.4 Applicability of Weibull model to predict strength of MEMS structures 12

2.5 Three-parameter Weibull distribution applied to material strength . . . 14

3 Generalized Finite Weakest Link Model for Material Failure **17**

3.1 Failure criterion for representative material element 18

3.2 Parameters contributing to random structural strength 20

3.2.1 Material tensile strength 20

3.2.2 Local dimensionless stress 22

3.3 Proposed expression for elemental and structural failure probability . . . 23

4 Comparison of Failure Statistics Models with Experimental Data **25**

4.1 Finite weakest link model 26

4.1.1 Distribution of notch geometry parameters 27
4.1.2 Stochastic elastic analysis of near-tip stress field 28
4.1.3 Calibration of distribution function for random material strength 32
4.2 Two-parameter Weibull model 34
4.3 Three-parameter Weibull model 35
4.4 Discussion 37

5 Extrapolations for Different Loading Configurations and Mean Size Effect 46
5.1 Analysis procedure 46
5.2 Predictions by Weibull distributions and comparison to present model . 50
5.3 Mean Size Effect 53

6 Conclusion 59

Bibliography 61

List of Tables

4.1 Calibrated statistical parameters of the finite weakest link model 32
4.2 Calibrated statistical parameters of the two- and three-parameter Weibull distributions 34

List of Figures

1.1 Measured strength histogram of MEMS materials, presented on the Weibull scale: a) single-crystal silicon [1]; b) hydrogen-free tetrahedral amorphous carbon (ta-C) [2]; c) poly-Si [3] 3
3.1 Tension specimen configuration 18
3.2 Representative element in a tension specimen 19
4.1 Measured strength histogram of poly-Si tensile specimens under uniaxial tension 26
4.2 Comparison of measured histogram of critical flaw depth and fitted distribution of V-notch depth 28
4.3 Portion of half-element FE model used for computation of near-tip stress field. The full model has width:length ratio of 10:1, so only the left end is shown. 29
4.4 Simulated tensile stress profile along notch ligament. 30
4.5 Probability distribution of dimensionless stress in V-notch 31
4.6 Finite weakest link models calibrated for the two sets of experimental results: a) calibrated for strength histogram of 20µm gauge-length specimens; b) calibrated for strength histogram of 70µm gauge-length specimens. 39
4.7 Prediciton of strength histograms by finite weakest link model: a) strength histogram of 20µm gauge-length specimens, predicted by model calibrated for 70µm gauge-length specimens; b) strength histogram of 70µm gauge-length specimens, predicted by model calibrated for 20µm gauge-length specimens. 40

4.8 Two-parameter Weibull distributions calibrated for the two sets of experimental results: a) calibrated for strength histogram of 20µm gauge-length specimens; b) calibrated for strength histogram of 70µm gauge-length specimens. 41
4.9 Prediciton of strength histograms by two-parameter Weibull distribution: a) strength histogram of 20µm gauge-length specimens, predicted by model calibrated for 70µm gauge-length specimens; b) strength histogram of 70µm gauge-length specimens, predicted by model calibrated for 20µm gauge-length specimens. 42
4.10 Three-parameter Weibull distributions calibrated for the two sets of experimental results: a) calibrated for strength histogram of 20µm gauge-length specimens; b) calibrated for strength histogram of 70µm gauge-length specimens. 43
4.11 Prediciton of strength histograms by three-parameter Weibull distribution: a) strength histogram of 20µm gauge-length specimens, predicted by model calibrated for 70µm gauge-length specimens; b) strength histogram of 70µm gauge-length specimens, predicted by model calibrated for 20µm gauge-length specimens. 44
4.12 Design strengths for poly-Si structure of various gauge lengths under uniaxial tension, corresponding to demanded reliability: a) $n = 1$ ($L_g =$ 0.4µm); b) $n = 5$ ($L_g = 2$µm); c) $n = 50$ ($L_g = 20$µm); d) $n = 500$ ($L_g = 200$µm); e) $n = 5000$ ($L_g = 2000$µm). 45
5.1 Configuration of poly-Si beam under three-point bending condition. Structural failure is initiated by fracture at one of the surface grooves. 47
5.2 Predicted strength histograms for poly-Si beams of various gauge lengths under flexural bending: a) $n = 12$ ($L_g = 4.8$µm); b) $n = 25$ ($L_g = 10$µm); c) $n = 50$ ($L_g = 20$µm); d) $n = 100$ ($L_g = 40$µm); e) $n = 200$ ($L_g = 80$µm). 57
5.3 Predicted mean size effect curve for poly-Si bars under uniaxial tension. 58

Chapter 1

Introduction

Polycrystalline silicon (poly-Si) is the dominant material used for fabrication of surface micromachined MEMS devices [4, 2]. Despite displaying average tensile strength considered to be higher than that of steel [4, 5], poly-Si shows a high variability of strength due to random heterogeneity of defects in its microstructures [6]. Without intrinsic toughening mechanisms, failure in poly-Si is controlled by flaws that are only tens of nanometers in size [4]. Moreover, it has been shown that the fracture failure of poly-Si is often governed by processing-induced surface defects rather than defects within the volume. Experiments further confirmed that tensile strength measured in micrometer-scale poly-Si tensile bars scaled with the length of specimens instead of the width, suggesting that fracture strength is associated more likely with the density of flaws occurring on the sidewalls rather than throughout the entire volume of the structure [7].

An intuitive response to this problem would be to improve fabrication process to produce silicon materials with "lowest possible bulk, surface, and edge cyrstallographic defect density to minimize potential regions of stress concentration", as already proposed by Peterson in 1982 [8]. Yet, eliminating processing-induced defects is not an easy task to accomplish. Efforts were also made to explore alternative materials for MEMS devices, including silicon carbide, ultrananocrystalline diamond, and hydrogen-free tetrahedral amorphous carbon. Fracture strength in these materials were, however, still observed to scale inversely with structure size, and fabrication-induced roughness was found to be a main contributing factor [2].

It is shown that the existence of randomly sized process-induced defects will inevitably lead to a high variability of fracture strength in poly-Si that cannot be tolerated in high-risk applications. Performance of reliability analysis is thus crucial in order to capture the "worst-case scenarios", and this was proposed to be accomplished through proof testing of MEMS devices [4]. However, since MEMS devices is typically designed against a failure probability on the order of 10^{-4} or lower [9], experimental determination of a target strength would require a large amount of testings, which can be expected to impose a challenge on structural reliability analysis. Early histogram testing of MEMS materials only involved a small number of specimens (less than 20 specimens measured per histogram [3]), mainly due to the limitation of testing procedures available at the time. Such a small number of specimens clearly does not suffice for the determination of a design strength required for a highly-reliable MEMS structure. Recent development of a slack-chain tester at the Sandia National Laboratories has allowed sequential tension tests to be efficiently performed on a much larger number of specimens ($\sim$1000 specimens [10, 5]). Nonetheless, it is still cost prohibitive to experimentally determine the strength corresponding to a failure probability as low as 10^{-4}, as it would likely require $\sim 10^5$ specimens to be prepared and tested to obtain a single strength histogram. Furthermore, since most experimental platforms are designed for specimens of a specific size, geometry, and loading configuration, a purely experimental analysis of structure reliability would necessitate the fabrication of many different testing platforms in order to measure the failure probability of MEMS structures subjected various kinds of loading conditions. Since this is apparently unfeasible, it is critical to understand the probabilistic failure of MEMS devices from a fundamental perspective.

Failure statistics of MEMS structures are commonly described by probabilistic models based on classical Weibull statistics, which is shown to effectively describe the probabilistic failure of brittle materials [11, 12, 13]. However, extensive histogram testings of MEMS materials have shown a deviation of the measured failure probability distribution from the form of a two-parameter Weibull distribution. For example, the three strength histograms displayed in Fig.1.1 clearly suggests that the histogram cannot be optimally fitted by a straight line on the Weibull scale. This deviation from the two-parameter Weibull distribution is most significant in the lower-probability region of the histogram, which contains the target failure probability demanded for a reliable MEMS

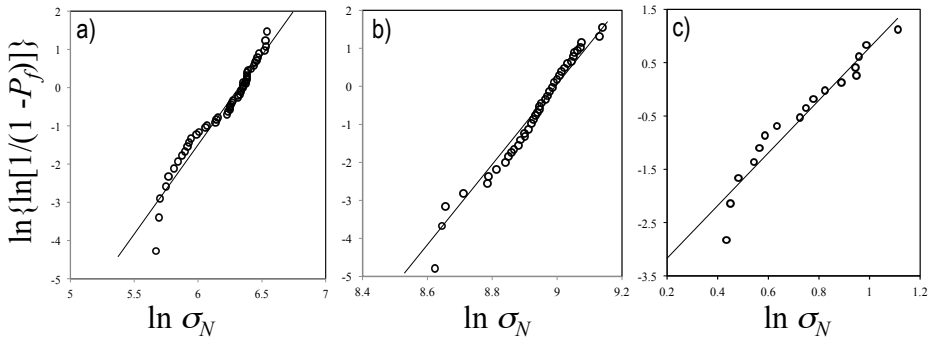

Figure 1.1: Measured strength histogram of MEMS materials, presented on the Weibull scale: a) single-crystal silicon [1]; b) hydrogen-free tetrahedral amorphous carbon (ta-C) [2]; c) poly-Si [3]

structure, and proves that the Weibull distribution cannot be applied to reliably describe failure statistics of materials used in MEMS structures. A popularly considered remedy to this issue is by adjusting the classical two-parameter Weibull distribution to a three-parameter Weibull distribution will a minimum threshold strength, with which an improved fitting of histogram data can be achieved [5, 6]. Yet, recent studies have indicated theoretical deficiencies of the three-parameter Weibull distributions due to its predicted scaling of structural strength with structure size, while the imposed threshold value is also questionable from a physical standpoint [14, 15]. In general, the existing probabilistic models for quasibrittle structures such as poly-Si are empirical in nature, and thus cannot effectively serve as theoretical tools for prediction of structural reliability in MEMS applications.

The main objective of this research is to formulate a robust probabilistic model to describe strength distribution of poly-Si MEMS structure. The proposed model is designed to be a generalized model applicable for structures both within and beyond the applicable range of the classical Weibull model, and thus is capable of predicting failure statistics for poly-Si structures across a broad range of geometry and loading configurations. The thesis is organized as follows: Chapter 2 reviews the two- and three-parameter Weibull statistical model, their fundamental assumptions, and applicability in modeling failure statistics of poly-Si MEMS structures; Chapter 3 presents

a generalized weakest link model for probabilistic failure of structures with positive geometry; Chapter 4 compares the present model with existing experimental data on the strength distribution on poly-Si MEMS structures; Chapter 5 demonstrates the prediction of failure statistics of MEMS structures under different loading configurations, and investigates the relationship between the mean size effect curve and the probability distribution of structural strength for MEMS devices.

Chapter 2

Weibull's Weakest Link Model for Material Strength

As a motivation for the development of a new model for failure statistics of quasi-brittle MEMS structures, it is necessary to first review details of the classical Weibull's weakest link model, the functional form of which is also commonly referred to as the two-parameter Weibull distribution. Weibull's model is perhaps the most widely used probabilistic model for brittle material strength, and has been shown to effectively provide optimum fit for strength histogram of materials such as fine-grain ceramics and fatigue-embrittled metals [11, 12, 13].

2.1 Formulation of Weibull's model

Weibull's weakest link model essentially states that a structure would fail under a load control condition once one representative material element fails. In other words, the probability of the survival of the entire structure would be the joint probability of the survival of all the representative material elements in the structure. Structures of such types are often referred to as being of positive geometry. Commonly seen examples of such structures include bars under uniaxial tension, beams under flexural loading, and plates under biaxial bending.

A general relationship can be established between the overall failure probability of the structure P_f and the failure probability of each representative material element P_1

by the joint probability theorem, i.e.:

$$P_f(\sigma_N) = 1 - \prod_{i=1}^{N} \{1 - P_1 [\sigma_N s(x_i)]\} \tag{2.1}$$

where $\sigma_N = c_n P_m / bD$ = nominal strength of the structure, P_m = load capacity of the structure, D = characteristic size of the structure, b = width of the structure in the transverse direction, c_n = a constant such that σ_N carries some physical meaning, e.g. the maximum elastic stress in the structure in the absence of stress concentration, N = the number of representative material elements in the structure, $s(x_i)$ = dimensionless stress field such that $\sigma_N s(x_i)$ is equal to the maximum elastic principal stress in the ith material element. It must be noted that Eq.(2.1) is based on the fundamental assumption that failure process of individual material elements will not influence each other, and therefore the strength of each element can be statistically treated as an independent random variable.

Eq.(2.1) can be rewritten in a logarithm form as:

$$\ln [1 - P_f(\sigma_N)] = \sum_{i=1}^{N} \ln\{1 - P_1 [\sigma_N s(x_i)]\} \tag{2.2}$$

A key consideration made in Weibull's analysis is that the number of representative material elements, N, is very large. As N becomes large, only the far-left tail of the failure probability distribution of an individual material element, P_1, will have a significant impact on the failure probability of the entire structure, P_f. By also considering that $\ln(1 - x) \approx -x$ $(x \to 0)$, Eq.(2.2) can then be rewritten in the following form for a structure containing a very large number of representative elements:

$$\ln[1 - P_f(\sigma_N)] = -\sum_{i=1}^{N} P_1[\sigma_N s(x_i)] \tag{2.3}$$

According to extensive histogram testing conducted on various engineering materials, including porcelain, cotton fabrics, wood, plaster-of-Paris, and portland cement [11], Weibull further discovered that, in order to fit the test data, the far-left tail of $P_1(x)$ should follow a power law, i.e. $P_1(x) = (x/s_0)^m$, where s_0 and m are material constants, now commonly referred to as the scale parameter and Weibull modulus (or shape parameter), respectively. Combining this observation with the previously stated

condition that N is a very large number, in which case the summation is equivalent to a volume integral, we can express Eq.(2.3) as:

$$\ln[1 - P_f(\sigma_N)] = -\sum_{i=1}^{N} \left(\frac{\sigma_N s(x_i)}{s_0} \right)^m \approx -\int_V \left(\frac{\sigma_N s(x)}{s_0} \right)^m \frac{dV(x)}{l_0^{n_d}} \tag{2.4}$$

hence ultimately leading to the commonly-seen form of the two-parameter Weibull distribution:

$$P_f(\sigma_N) = 1 - \exp\left[-C(\sigma_N/s_0)^m\right] \tag{2.5}$$

where $C = l_0^{-n_d} \int_V s^m(x) dV(x)$. In the above expressions, l_0 = characteristic size of the representative material element, and n_d = number of spatial dimension of the structure considered in the model, e.g. $n_d = 1$ for a bar under uniaxial loading, and $n_d = 2$ for a plate under biaxial bending.

2.2 Weibull distribution in extreme value statistics

The distribution function stated in Eq.(2.5) was independently proposed by Weibull based on the formulation procedure summarized above, along with empirical observations made according to a large amount of experimental testings. Weibull later also proposed the application of the Weibull distribution to a wide field of problems, some even outside of material mechanics, including statures for adult males and breadth of beans [12]. However, from a purely statistical viewpoint, the Weibull distribution described in Eq.(2.5) belongs to the class of extreme value distribution functions, which was mathematically derived earlier, along with the Gumbel and Fréchet distribution, by Fisher and Tippet based on the postulate of stability [16]. The analysis performed by Fisher and Tippet will be reviewed below.

For a sample with a size $m{\cdot}n$, the maximum member in the sample could be considered as the maximum member in n samples each containing the maximum member in a sample of the size m. If an asymptotic form of distribution exists for the sample maximum, both of the aforementioned cases will approach the limiting form as m is indefinitely increased. The limiting form of the extreme value must therefore allow for a similar distribution to be observed for the maximum member of a sample of the size n, when n is infinitely increased. Provided that P is the probability that an observation is

less than x, i.e. the cdf of the given distribution, the probability that the greatest of a sample n is less than x would be expressed as P^n. According to the stability postulate, the functional form of P and P^n shall be similar, except for a linear transformation, i.e.:

$$P^n(x) = P(a_n x + b_n) \tag{2.6}$$

Fisher and Tippet stated that, by obtaining solutions for this functional equation, all possible options of limiting forms can be derived. It was concluded that Eq.(2.6) is satisfied under one of the following conditions:

1. $a_n = 1$,
$$P^n(x) = P(x + b_n) \tag{2.7}$$

2. $a_n \neq 1$, $P^n = P$ when $x = b_n/(1 - a_n)$. For $P^n = P$ to be satisifed, $P = 0$ or 1, which are the two extremes of probabilities, expected to occur at $x = 0$ for distribution of random variables with physical meanings. Hence, in this case, $b_n = 0$ and
$$P^n(x) = P(a_n x) \tag{2.8}$$

Under the first possible condition, Eq.(2.7) can be further rewritten in a logarithm form as:

$$\log n + \log(-\log P(x)) = \log(-\log P(x + b_n)) \tag{2.9}$$

which would suggest that the expression $\log(-\log P(x)) - x \log n/b_n$ would either be a constant or periodic with a period of b_n.

Furthermore, the initially defined functional relation yields $P(x + b_{mn}) = P^{mn}(x) = P^m(x + b_n) = P(x + b_m + b_n)$, which means that

$$b_{mn} = b_m + b_n \tag{2.10}$$

holds for all values of m and n. Suppose that b_n is an analytic function of n, which would exclude the aforementioned possibility of periodic solution. By taking derivative of Eq.(2.10) about m and n, respectively, the following relations would hold:

$$n b'_{mn} = b'_m \tag{2.11}$$

$$m b'_{mn} = b'_n \tag{2.12}$$

which together would essentially suggest that $b'n = c/n$, where c is a constant. Hence,

$$b_n = c \log n + d \tag{2.13}$$

where d is another constant. Yet, noting that $b_1 = 0$, it can be concluded that $d = 0$. Since $\log(-\log P(x)) - x \log n/b_n = \text{constant}$, this can be written as:

$$\log(-\log P(x)) = \frac{x}{c} + C \tag{2.14}$$

where C is a constant. Noting that $P(x)$ should increase with x, it is clear that c must be negative. Fisher and Tippet concluded that the limiting form of Eq.(2.13) therefore is that of $-\log(-\log P_x) = x$. The distribution of the maximum in a sample of the size n would then be:

$$-\log(-\log P_x) = x - b_n = x - \log n \tag{2.15}$$

This is the solution to Eq.(2.6) under the first possible condition.

Next, analyze the second condition under which Eq.(2.6) holds. As described in Eq.(2.8), $P^n(x) = P(a_n x)$, hence $P(a_{mn}x) = P^{mn}(x) = P^m(a_n x) = P(a_m a_n x)$, which would give:

$$a_{mn} = a_m \cdot a_n \tag{2.16}$$

Similar to the previous analysis procedure leading to the first solution of limiting forms, take derivative of Eq.(2.16) about n and m, respectively, to obtain

$$m a'_{mn} = a_m a'_n \tag{2.17}$$

$$n a'_{mn} = a'_m a_n \tag{2.18}$$

which would together suggest that $a'_n/a_n = -1/kn$, where k is a constant. Therefore we may express a_n as

$$a_n = n^{-1/k} \tag{2.19}$$

satisfying the basic condition that $a_1 = 1$. Again, similar to the procedure leading to Eq.(2.9), a logarithm form of Eq.(2.8) may be expressed as:

$$\log n + \log(-\log P(x)) = \log(-\log P(a_n x)) \tag{2.20}$$

Once again excluding the possibility of periodic solution, it can be concluded that

$$\log(-\log P(x)) = -k \log x + B \tag{2.21}$$

$$-\log P(x) = Ax^{-k} \tag{2.22}$$

where B and A are two constants.

If $P = 0$ when $x = 0$, k will be positive, and $P(x)$ should have the functional form

$$P(x) = e^{-x^{-k}} \tag{2.23}$$

If $P = 1$ when $x = 0$, k will be negative, and $P(x)$ should have the functional form

$$P(x) = e^{-(-x)^{k}} \tag{2.24}$$

The three possible forms of solutions to Eq.(2.6) are thus stated in Eqs.(2.15), (2.23), and (2.24). Based on these solutions, the possible forms of pdf for the asymptotic distribution of maximum value can be written as:

I. $dP = e^{-x-e^{-x}}dx$

II. $dP = \frac{k}{x^{k+1}} e^{-x^{-k}} dx \qquad (x \geq 0)$

III. $dP = k(-x)^{k-1} e^{-(-x)^{k}} dx \qquad (x \leq 0)$

Exactly in this order of enumeration, the three classes of limiting curves are now referred to as the extreme value distribution (for the maximum) of type I, type II, and type III. These three types of extreme value distributions are also commonly referred to as the Gumbel, Fréchet, and Weibull distributions, respectively. These three classes of distribution for maximum values can be easily transformed to corresponding forms of distribution functions for minimum values, based on symmetry:

I. $dP = e^{x-e^{x}}dx$

II. $dP = \frac{k}{(-x)^{k+1}} e^{-(-x)^{-k}} dx \quad (x \leq 0)$

III. $dP = kx^{k-1} e^{-x^{k}} dx \quad (x \geq 0)$

Prior to the publication of Fisher and Tippet's 1928 paper presenting the three classes of extreme value distributions, similar work was also completed by Maurice Fréchet in 1927 [17], in which he obtained one of the three aforementioned asymptotic distribution later found independently by Fisher and Tippet. Unfortunately, perhaps due to the fact that it was published in a remote Polish journal, Fréchet's paper did not gain the recognition equivalent to that of Fisher and Tippet's paper [18].

It must also be noted that the Gumbel and Fréchet distributions, though also belonging to the class of extreme value distribution functions, cannot be applied to describe the strength of material. This is due to the fact that these distributions, as can be seen from the functional form, govern the minimum as $\sigma \to -\infty$ and the distribution will have infinite negative tail, which would be nonphysical for material behavior.

2.3 Prediction of nominal strength using Weibull model

With the physical implications of the two-parameter Weibull distribution reviewed, now consider applying the model to describe the scaling of strength in geometrically similar structures. Given a set of geometrically similar structures of different sizes D subject to identical loading conditions, the elastic dimensionless stress field generated in all structures would qualitatively be the same, regardless of structure size. Hence the constant C term in Eq.(2.5) can be expressed in terms of a dimensionless coordinate $\xi = x/D$, and rewritten as follows:

$$C = l_0^{-n_d} \int_V s^m(x) dV(x) = \Psi \left(\frac{D}{l_0} \right)^{n_d} \tag{2.25}$$

where $\Psi = \int_V s^m(\xi) dV(\xi)$. Additionally, for the overall structure, the mean nominal strength can be determined simply by computing the expected value of σ_N in the probability space:

$$\bar{\sigma} = \int_0^1 \sigma_N(P_f) dP_f = \int_0^\infty \left[1 - P_f(\sigma_N)\right] d\sigma_N \tag{2.26}$$

By substituting Eq.(2.25) into Eq.(2.26), we have the following expression for the mean nominal structural strength:

$$\bar{\sigma} = s_0 \Gamma(1 + 1/m) l_0^{n_d/m} \Psi^{-1/m} D^{-n_d/m} \tag{2.27}$$

where $\Gamma(x)$ = Eulerian gamma function. Eq.(2.27) suggests that the mean nominal strength of the structure decreases with an increasing structure size, since $\bar{\sigma} \propto D^{-n_d/m}$. This relation between the size and strength of the structure is the Weibull size effect, which is often used to explain the size dependence of strength in materials.

It is also worthwhile to note that the characteristic length of the representative material element, l_0, is not included in the expression of mean nominal strength of the structure, as shown in Eq.(2.27). This is in accordance with the assumption made in Weibull's analysis that the number of representative material element is very large and thus the size of each element is essentially negligible when compared to the size of the overall structure. Consequentially, we have the power-law scaling of structural strength unaffected by the characteristic length of individual representative elements.

Later in Chapter 5 of this study, the mean size effect as predicted by the two-parameter Weibull distribution will be compared in detail with the size effect predicted by the proposed model.

2.4 Applicability of Weibull model to predict strength of MEMS structures

As discussed above, Weibull's weakest link model for material strength is based on the following fundamental assumptions:

1. Structural failure is triggered by the failure of one representative material element, i.e. a weakest link model of structural failure;

2. The strength of individual material elements are treated as random variables that are statistically independent, i.e. the failure of process of one element will not influence that of another element;

3. The probability distribution of representative element strength should have a far-left tail in the form of a power law;

4. The number of representative material elements in the structure is very large, so that the size of the element is negligibly small in contrast to the structure size.

In order to correctly apply the Weibull model to describe the probabilistic failure of a structure, it is crucial to verify the validity of each assumption stated above. As discussed earlier, the weakest link relation is valid for structures of positive geometry, and therefore is appropriate for modeling poly-Si MEMS structures under loading configurations such as uniaxial tension and flexural bending, which are the two cases later investigated in this study. The statistical independence of individual material element strength can be generally satisfied by selecting a representative element with a size l_0 larger than the autocorrelation length of the random strength field.

The power-law tail of the representative material element strength distribution was originally proposed by Weibull according to results of experimental testings. A physical justification for the power-law tail was first proposed by Freudenthal[19], assuming that the distribution of material flaw sizes followed an inverse power law and also neglecting material heterogeneity and flaw interactions. A more comprehensive theoretical justification for Weibull's assumption has been developed recently [20, 13, 15], in which the power-law tail of material strength distribution was explained by combining transition state theory and a multiscale statistical model. Considering nanocrack propagation through atomic lattices, the jump of a nanocrack over a single atomic bond would be considered as the transition between two metastable states. Based on Maxwell-Boltzmann distribution of atomic thermal energies, the cdf of the strength strength is proven to contain a power-law tail with exponent of 2 at the nano-scale [15]. The size of the exponent will increase when upscaled through the hierarchical structure of the material, which is reflected as the Weibull modulus for the material at the structural scale.

The final assumption of Weibull's model requires that the size of material inhomogeneities is sufficiently small in order to be negligible compared to the size of the entire structure. As shown in the earlier derivation of the Weibull distribution function, this assumption is critical for simplifying the functional form of material strength distribution to what was shown in Eq.(2.5). This condition is not automatically satisfied for all structures, yet the assumption is often unmentioned when applying Weibull distribution to model material strength. In many cases, the structure does not contain a large number of representative material element, and the use of a Weibull distribution to model the structure strength is clearly unjustifiable.

Recent experimental observations have shown that process-induced sidewall grooves are the main source of the variability in the strength of poly-Si tensile bars. This type of surface defects serve as stress concentrators, from which the failure of the structures are expected to initiate [6, 5]. It is therefore reasonable to consider each sidewall groove as a representative material element in the weakest link model. A tensile specimen with a length of 20μm was observed to contain ∼100 sidewall grooves [5]. Based on this result, it can be assumed that for typical MEMS structures with characteristic length no larger than 0.1mm, the number of representative material element is expected to be less than 1000, which is at least an order of magnitude less than the required number for the Weibull model to be applicable.

The insufficient number of representative elements in the MEMS structures shows that the probability distribution of the structural strength cannot be properly described by Weibull's model, and this accounts for the fact that an optimal fit of two-parameter Weibull distribution cannot be achieved for measured strength histograms of MEMS structures. Additionally, the randomness of the sidewall grooves geometry, which leads to the random local stress field along the sidewall, cannot be directly incorporated in the expression of the Weibull model. Due to these inadequacies, the classical Weibull model is invalid for describing the reliability of MEMS structures, and an alternative model is necessary to determine the failure statistics of the poly-Si material.

2.5 Three-parameter Weibull distribution applied to material strength

A strength histogram described by two-parameter Weibull distribution will form a straight line on a Weibull scale plot with a slope of m, the Weibull modulus. Yet, experimentally obtained strength histogram of materials, as shown earlier in Fig.1.1, sometimes exhibit a kink separating two segments, and thus the histogram clearly cannot be optimally fitted by a straight line.

As a remedy for the divergence of the classic two-parameter Weibull distribution from the probability distribution of material strength, the three-parameter Weibull distribution is popularly used as an alternative model. The three-parameter Weibull distribution adjusts the classic Weibull model shown in Eq.(2.5) by introducing a finite

strength threshold value under which the material structure will never fail. The functional form of this distribution can thus be written as:

$$P_f(\sigma_N) = 1 - \exp\left[-C\left(\frac{\langle\sigma_N - \sigma_0\rangle}{s_0}\right)^m\right] \tag{2.28}$$

of which m and s_0 are the Weibull modulus and scaling parameters, respectively, and σ_0 = strength threshold corresponding to zero failure probability of the material, regardless of structure size. When failure statistics described by three-parameter Weibull distribution is plotted on the Weibull scale, the histogram will display a far-left tail asymptotically approaching the vertical line corresponding to $\sigma_N = \sigma_0$, a linear far-right tail resembling the form of two-parameter Weibull distribution, and a curved transition zone in between. Hence in many cases, the parameters can be calibrated to visually provide optimum fitting of some strength histograms that otherwise deviate from the two-parameter Weibull distribution.

However, this type of distribution has recently been shown theoretically unsound for strength statistics of brittle and quasibrittle structures, as it contains the following flaws:

1. The strength threshold applied is physically unjustifiable. As theoretically justified based on the transition state theory, the probability distribution of material strength should have a power-law with zero threshold [13, 15]. A non-zero threshold would contradict with this result, as it would be impossible for a finite threshold to suddenly appear following the change of structure size.

2. The model predicts an incorrect size effect on the mean structural strength at the large size limit [14].

In additional to the theoretical arguments invalidating the application of three-parameter Weibull distribution for material strength, extensive experimental testings have also shown that material strength histograms cannot always be optimally fitted by a three-parameter Weibull distribution. Histogram based on relatively large data sets will deviate from a three-parameter Weibull distribution, particularly in the extremely low and high probability range [13, 14].

As a type of distribution function commonly believed to effectively provide optimum fittings for probability distribution of material strength, including poly-Si MEMS

structures [5], the three-parameter Weibull distribution will later be compared in detail with the model presented in this study. The theoretical validity of the three-parameter Weibull distribution will also be carefully examined for the specific application of modeling failure statistics in poly-Si MEMS structures.

Chapter 3

Generalized Finite Weakest Link Model for Material Failure

Investigation of pre-existing sidewall flaws in poly-Si microstructure by atomic force microscopy (AFM) showed that the narrow grain boundary grooves generated by preferential etching are roughly V-shaped [5]. When modeling poly-Si tensile bar specimens, it is thus common to idealize the grooves as V-notches. When the specimen is subjected to uniaxial tension, as illustrated in Fig.3.1, a maximum value of applied stress, σ_N, is reached once crack propagation occurs in one of the V-shaped sidewall grooves. As discussed previously, this type of structures in which failure is triggered by the failure of one representative material element can be modeled with a weakest link model. The overall failure probability of the specimen can thus be calculated according to Eq.(2.1).

In this case, the function $P_1(x)$ in Eq.(2.1) represents the probability of localized crack propagation from one surface groove under an applied tensile stress. As previously mentioned, the number of representative material elements in typical MEMS structures is too small for the classic two-parameter Weibull distribution to be applicable. To properly model the failure statistics associated with specimens containing any finite number of representative material elements, it is necessary to obtain an expression for the entire function of an individual element's failure probability, $P_1(x)$, rather than only the far-left tail of the function. By considering structures to whose failure statistics the

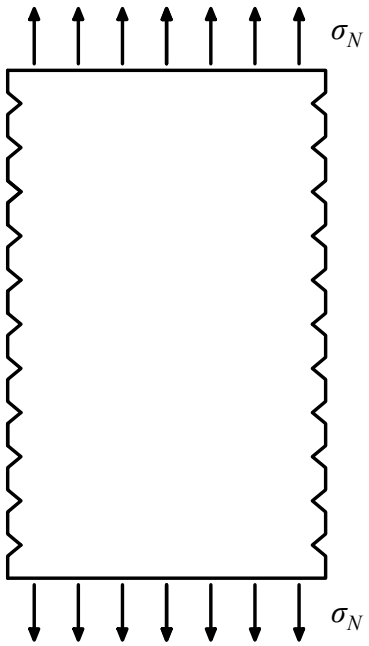

Figure 3.1: Tension specimen configuration

original Weibull's model were inapplicable, the present model can be interpreted as a generalization of the material strength model proposed by Weibull, and herein referred to as the finite weakest link model.

3.1 Failure criterion for representative material element

A fundamental requirement for computing $P_1(x)$ is to define a criterion for structural failure. In the case of this study, we consider that a localized crack would be initiated and begin propagation from one of the surface grooves, each idealized as a V-notch, once the average tensile stress $\bar{\sigma}$ of the near-tip region exceeds the tensile strength f_t of the material. The average tensile stress is defined as:

$$\bar{\sigma} = \frac{1}{r_c} \int_0^{r_c} \sigma_{yy}(x) dx \tag{3.1}$$

where $\sigma_{yy}(x)$ = elastic tensile stress along the notch ligament, as shown in Fig.3.2, and r_c = size of the selected near-tip region in which the average stress is computed.

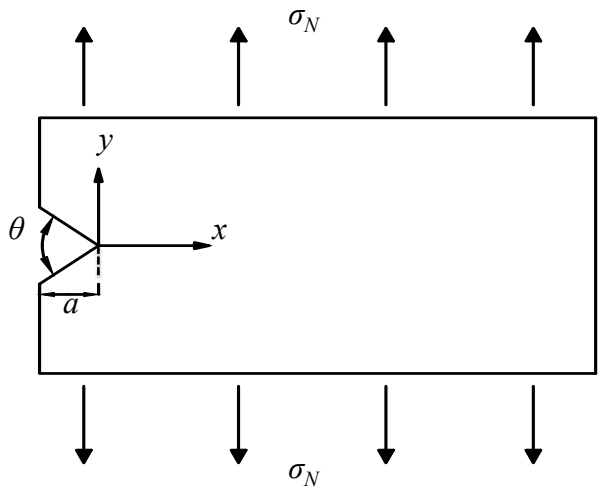

Figure 3.2: Representative element in a tension specimen

The averaging procedure applied here can be considered as a simplified version of the non-local approach that accounts for the interaction of the sub-scale damage inside the fracture process zone (FPZ) formed at the tip of the V-notch prior to crack propagation. With this simplification, it must be noted that the material tensile strength f_t considered in the failure criterion should be understood as the tensile strength of the material element, whose size is approximately equal to the FPZ size.

In this study, the size of the near-tip region is selected to be $r_c = 5$ nm, which is in general agreement with previous estimation of FPZ size in silicon [5, 21]. It must be noted that further determination of an exact value for r_c can be achieved through detailed atomistic calculations for the near-tip region. This would also help provide additional insights into the failure behavior of silicon crystals. As will be presented in detail later, the currently selected value of r_c is based on linear elastic finite element analysis of the representative material element containing a V-notch. It is clear that the specific choice of r_c will certainly influence the calibration of the probability distribution of the material tensile strength. However, as will be also clarified later, the qualitative behavior of the present model will not be affected by the chosen value of r_c, as long as it is selected within a reasonable range where the random distribution of $\bar{\sigma}$ can be properly reflected.

Given the failure criterion defined above, failure occurs when $\bar{\sigma} \geq f_t$. By further introducing a local dimensionless stress s, satisfying the relation $\sigma_N s = \bar{\sigma}$, we can state the failure probability of the representative material element as:

$$P_1(\sigma_N) = \text{Prob}(\sigma_N s \geq f_t) = \text{Prob}(f_t/s \leq \sigma_N) \tag{3.2}$$

3.2 Parameters contributing to random structural strength

In Eq.(3.2), both f_t and s are variables subjected to a certain level of randomness. Therefore, a necessary step towards evaluating $P_1(\sigma_N)$ would be to understand the probabilistic distribution of the material strength, f_t, and that of the local dimensionless stress, s.

3.2.1 Material tensile strength

Recent comprehensive studies on the strength statistics of quasibrittle materials have provided mathematical expressions for the probability distribution of material tensile strength [20, 13]. Generally, the strength distribution of a material element in a quasibrittle structure can be described by a Gaussian distribution with a Weibull tail grafted on the left at a point of the probability typically of about 10^{-4} to 10^{-3}. This grafted cumulative distribution function (cdf) can be mathematically expressed as:

$$P_{f_t}(\sigma) = 1 - e^{-(\sigma/s_0)^m} \qquad (\sigma \leq \sigma_{gr}) \tag{3.3}$$

$$P_{f_t}(\sigma) = P_g r + \frac{r_f}{\delta_G \sqrt{2\pi}} \int_{\sigma_{gr}}^{\sigma} e^{-(\sigma' - \mu_G)^2/2\delta_G^2} d\sigma' \qquad (\sigma \geq \sigma_{gr}) \tag{3.4}$$

where m = Weibull modulus (shape parameter), s_0 = Weibull scale parameter, μ_G = mean of the Gaussian core, δ_G = standard deviation of the Gaussian core, r_f = a scaling parameter required to normalize the cdf so that $P_{f_t}(\infty) = 1$, and finally, $P_{gr} = 1 - e^{-(\sigma_{gr}/s_0)^m}$ = probability at which the grafting occurs and the Weibull tail transitions to Gaussian core (the grafting probability). The parameter σ_{gr}, which corresponds to the tensile stress capacity at which grafting of the cdf takes place, will be referred to as the grafting stress. Additionally, the continuity of the probability density function, i.e. the first derivative of the cdf about σ, must be enforced at $\sigma = \sigma_{gr}$. This additional

condition is expressed as:

$$dP_{f_t}(\sigma)/d\sigma|_{\sigma=\sigma_{gr}^-} = dP_{f_t}(\sigma)/d\sigma|_{\sigma=\sigma_{gr}^+} \tag{3.5}$$

Without reviewing the full derivation of the grafted Gaussian-Weibull functional form of material strength distribution, the mathematical expression can be qualitatively interpreted as follows. When the size of the material element approaches the size of the FPZ, the failure behavior of the element would be quasi-plastic, and thus the strength of the material element could be calculated as the sum of strengths of all sub-scale material elements along the failure surface. According to the Central Limit Theorem, the sum of the individual sub-scale element strength $S = \sum_{i=1}^{n} \sigma_i$, where the subscale element strength σ_i would be each considered as an independent random variables with some well-defined mean and variance, ultimately converges to a normal distribution when $n \to \infty$. Furthermore, it is apparent that the far-left tail of the Gaussian distribution would extend to negative values of material strength, and hence must be rejected from a physical standpoint. As described in the previous chapter, recent studies have theoretically justified that the probability distribution of strength for all materials should have a power-law tail, regardless of the length scale of the material structure investigated [20, 13, 15].

Combining the functional form of material strength distribution described in Eqs.(3.3) and (3.4) with the basic form of weakest link model, as shown in Eq.(2.1), it is clear that once the structure contains a large number of material elements, the failure behavior would be more of a brittle manner, i.e. the failure statistics would generally match the classical two-parameter Weibull distribution. As a simple example, consider a material structure containing N_{eq} identical elements with the failure probability $P_1(\sigma_N) = \text{Prob}(f_t \leq \sigma_N s)$, and assume stress field in all representative material elements are uniformly distributed so that s can be taken as a constant. For the probability distribution of structure strength, the transition between Weibull tail and Gaussian core would occur at $P_f(\sigma_N s = \sigma_{gr}) = 1 - [1 - P_1(\sigma_{gr})]^{N_{eq}}$. When N_{eq} is increased, $P_f(\sigma_{gr})$ would be expected to increase accordingly. Once N_{eq} become large enough for the Gaussian core to be relatively unnoticeable on a Weibull plot of the material failure statistics, the structure becomes brittle enough for its failure probability to be accurately calculated based only on the Weibull tail, i.e. the classical two-parameter Weibull distribution

would be applicable for this structure.

To further illustrate this size effect, consider a specific case where $P_{gr} = 10^{-3}$ for the material, which would be considered a relatively high value. For a structure containing a single element, the Weibull tail only extends to $\ln[\ln(1/(1-P_{gr}))] = -6.9$ on a Weibull probability paper. Having the plot of the structural failure probability to be visually identical to a Weibull distribution perhaps would require $\ln[\ln(1/(1-P_f))] \geq 3$, which roughly corresponds to $N_{eq} \geq 2 \times 10^4$. Thus it can be concluded that any N_{eq} below this order of magnitude generally would not justify the use of two-parameter Weibull distribution to describe the strength statistics of the overall structure, as the Gaussian core is still non-negligible in the determination of failure probability.

3.2.2 Local dimensionless stress

In the expression of the failure probability of an representative element in a poly-Si structure, as stated in Eq.(3.2), the strength of the structure depends not only on the random tensile strength of the material, but also the random dimensionless stress depending on the geometry of the surface groove modeled as a V-notch. In this study, elastic stress field generated near individual V-notches are assumed to be non-interactive with each other. Based on this assumption, the dimensionless stress for a representative material element can be computed by considering only a single element itself, i.e. the strip of the specimen containing a V-notch on one of its sidewall, as shown earlier in Fig.3.2. Furthermore, it must be noted that sidewall grooves are expected to exist on the other side of the strip, but should not affect the near-tip stress field of the V-notch examined. As shown in Fig.3.2, of which the dimensions are proportionally scaled to that of an actual representative element in poly-Si, the width of a typical MEMS specimen (on the order of microns) is much larger than the depth of the V-notch (typically below 100 nm) and the overall size of the near-tip region. Thus it can be assumed that V-notches on opposite sidewalls are located too far apart to impact the near-tip stress field of each other.

Recent studies by Reedy et al.[5] have shown that variations in crystal orientation in silicons do not contribute significantly to the measured near-tip stress field in a columnar polycrystalline silicon microstructure. Therefore, randomness of crystal orientation will not be considered in this study, and the material will be modeled isotropically with a set

of elastic properties reflecting the behavior of a random aggregate of columnar silicon crystals. With this assumption, the only contributing factors to the dimensionless stress would be the random geometry of the V-notch located on sidewall of the strip.

The random geometry of a V-notch is essentially determined by two parameters: the notch angle θ and the notch depth a. By defining probability distribution functions for the geometric parameters according to previously obtained knowledge of surface groove geometry, stochastic analysis of the near-tip stress field can be performed to provide the probability distribution of the dimensionless stress, $F_s(x)$.

3.3 Proposed expression for elemental and structural failure probability

By considering the specific cases of randomness associated with the material element strength and the V-notch geometry, the failure probability of the representative material element, as stated in Eq.(3.2), can be further rewritten in detail:

$$P_1(\sigma_N) = \int_0^\infty P_{f_t}(x\sigma_N) f_s(x) dx \tag{3.6}$$

where $f_s(x) = dF_s(x)/dx$ = pdf of the dimensionless stress, s. In this study, $f_s(x)$ is numerically computed based on histogram of $F_s(x)$ obtained from stochastic simulations, and then P_{f_t} is the grafted cdf stated in Eqs.(3.3) and (3.4) with parameter calibrated to provide optimum fit of strength histogram experimentally measured for the specific material. Based on the aforementioned expression of $P_1(\sigma_N)$, the probability distribution of tensile strength for the entire tensile bar structure can then be expressed as:

$$P_f(\sigma_N) = 1 - \left[1 - \int_0^\infty P_{f_t}(x\sigma_N) f_s(x) dx\right]^{2n} \tag{3.7}$$

where $n = L/l_0$ = number of V-notches along one sidewall of the specimen. Note again that the expression in Eq.(3.7) basically states that the failure probability of each individual material element in the structure is statistically independent, and therefore together relates to the failure probability of the overall structure by the weakest link model. As previously mentioned, the statistical independence of individual element failure is validated by the fact that the V-notch has a size considerably larger than the

FPZ size, which is approximated to be on the same order of the autocorrelation length of random strength field for brittle and quasibrittle materials [13].

When the sidewall of a poly-Si specimen under uniaxial tension contains a large number of surface grooves, i.e. $n \to \infty$, an asymptotic form of $P_f(\sigma_N)$ can be derived, resembling the limit distribution for extreme value statistics. In this case, only the Weibull tail portion of $P_1(\sigma_N)$ is needed to determine $P_f(\sigma_N)$, and failure is expected to occur at a relatively small value of σ_N. Note that in this case, Eq.(3.3) can be approximated as $P_{f_t}(\sigma) \approx (\sigma/s_0)^m$ for a small value of σ approaching zero. Using this simplified form, Eq.(3.6) can be expressed as:

$$P_1(\sigma_N) = \int_0^\infty \left(\frac{\sigma_N x}{s_0}\right)^m f_s(x)dx = M_m \left(\frac{\sigma_N}{s_0}\right)^m \tag{3.8}$$

where $M_m = \int_0^\infty x^m f_s(x)dx = m$th moment of the distribution function for dimensionless stress, $F_s(x)$. Hence, by substituting Eq.(3.8) into Eq.(3.7), we can see that the finite weakest link model converges, at the large-size limit, to the classical Weibull distribution:

$$P_f(\sigma_N) = 1 - \exp\left[-2nM_m \left(\sigma_N/s_0\right)^m\right] \tag{3.9}$$

It can be seen from Eq.(3.9) that the Weibull tail of the strength histogram of structure, when plotted on a Weibull scale, will always be a straight line with a slope of m. Thus the Weibull modulus can be easily calibrated directly from a sufficiently large set of test data, where the far-left tail is reflected in the low probability region.

Contrarily, when there is only a finite number of representative element present in the structure, i.e. the number of surface grooves along the specimen sidewall is much below the demanded order of $\sim 10^4$, the strength distribution of the structure is expected to deviate from the two-parameter Weibull distribution. This transition from non-Weibullian to Weibull strength distribution as a function of structure size would lead to a size effect on the mean structural strength that can be expected to have a form more complex than that of the classical Weibull size effect. As will be presented in detail later on, the predicted size effect can be inversely applied to verify the accuracy of the failure probability model. In this sense, the deviation of measured mean size effect curve from the Weibull size effect will also confirm the deviation of the structural strength cdf from the form of a two-parameter Weibull distribution.

Chapter 4

Comparison of Failure Statistics Models with Experimental Data

High-throughput testing methods have been recently developed to efficiently test a large numbers of poly-Si tensile bars. With suitable streamlining and automation of experimental procedure, the developed testing methods allows for material strength to be measured for thousands of specimens, which consequentially provides more detailed strength histograms for an improved understanding of strength statistics in MEMS devices. Micrometer-scale poly-Si tensile bars of two different gauge lengths were tested using two high-throughput methods [5], and the results are presented in Fig.4.1. The on-chip method, developed by Hazra et. al [22], were used to measure 231 specimens of 70 µm gauge length. This method uses an on-chip chevron thermal actuator to apply stress to a self-aligning tensile specimen via a prehensile grip mechanism. Through reduction of voltage, the cooling of thermal actuator generates monotonic tensile stress on the tested specimens, ultimately leading to fracture. The slack-chain method, developed by Boyce [10], applies an external load to a chain of specimens by a custom-built probe station, and was used to measure 1287 specimens with a gauge length of 20 µm. The specimens tested with these two methods all have a nominal width of 2µm.

In this chapter, the three failure statistics models of interest — the proposed finite-weakest link model, the two-parameter Weibull distribution, and the three-parameter

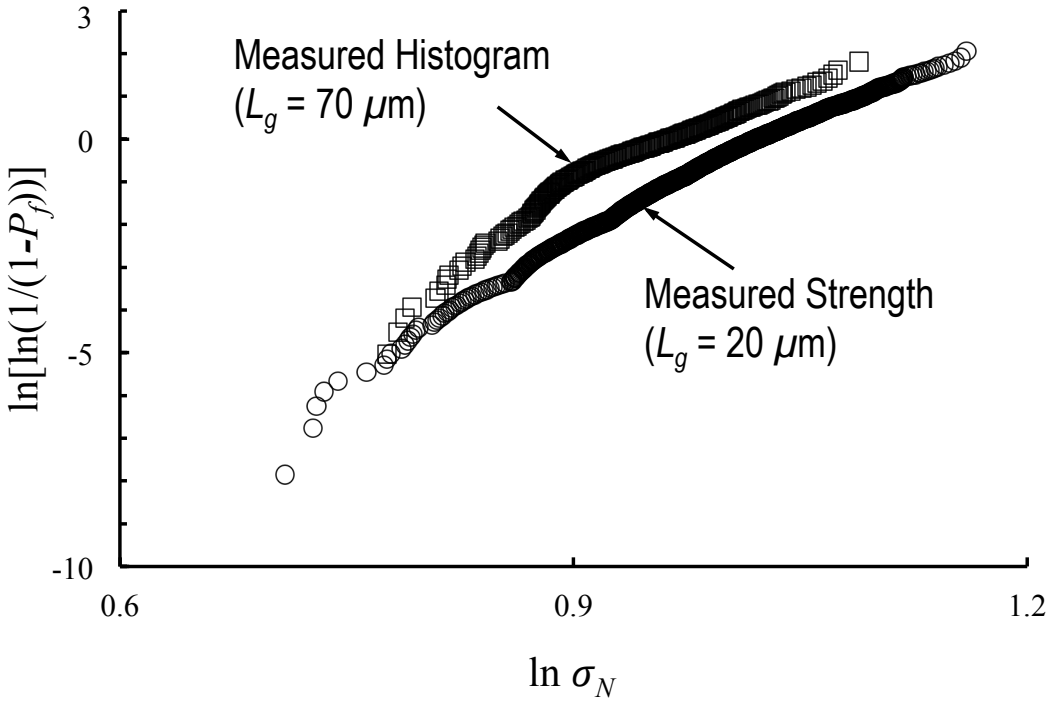

Figure 4.1: Measured strength histogram of poly-Si tensile specimens under uniaxial tension

Weibull distribution — are each calibrated according to the measured strength histograms, and then applied to predict failure probability of poly-Si tensile bars across a large range of specimen sizes.

4.1 Finite weakest link model

The presented general finite weakest link model will be fitted according to experimental data of tensile testing on poly-Si specimens. For a tensile specimens tested with the slack-chain method, the gauge length was measured to be 20 µm, while approximately 100 surface grooves were measured on the sidewalls of each specimen — giving a total of 50 on each sidewall. Specimens measured by the on-chip method, with gauge length of 70 µm, were assumed to have surface grooves distributed in a similar density, and thus

estimated to have 175 grooves on each sidewall. As previously discussed, the failure of individual representative elements in a poly-Si tensile bar is assumed to be independent of each other. The random dimensionless stress, s, in an element will thus be calculated by investigating a single element rather than the overall structure, i.e. consider only a strip of specimen with a V-notch placed along a 400 nm sidewall, subject to a unit tensile stress ($\sigma_N = 1$ (GPa)) uniformly distributed along its top and bottom ends. As explained earlier, the width of the strip is 2 µm, too large for near-tip stress fields on opposite sidewalls to interact with each other. Thus a V-notch will only need to be placed on one of the sidewalls of the modeled representative element model to study the near-tip elastic stress field.

4.1.1 Distribution of notch geometry parameters

As mentioned in the previous chapter, the randomness of the near-tip stress field is governed by the geometry of the V-notch, which is determined by two parameters, notch angle θ and notch depth a. Histogram of the effective critical flaw depths in poly-Si specimens were generated according to measurements of 1287 tensile bars, showing that flaw depths typically ranged between 25 and 61 nm. Based on the histogram, the notch depth a was assumed to follow a Type III extreme value distribution for the maximum value, with the cdf expressed as:

$$F_a(x) = \exp\left[-\left(\frac{\langle 62 - x\rangle}{28}\right)^{6.5}\right] \tag{4.1}$$

where $\langle x\rangle = max(x, 0)$. Comparison of the measured histogram of the notch depth and the fitted distribution function is presented in Fig. 4.2. The size of the notch angle, θ, was assumed to follow a uniform distribution bounded between 20° and 140°, and thus the cdf will be written as:

$$F_\theta(x) = \frac{x - 20}{120} \tag{4.2}$$

It is noted that the assumed distribution function for the notch depth extends to negative values, which is physically impossible, since it would suggest a negative notch depth. However, this tail only extends to $F_a(0) = 6.7 \times 10^{-77}$, i.e. a negative notch depth value is expected to occur once in every 1.49×10^{76} samples. Such a short tail can essentially be neglected in the sampling process.

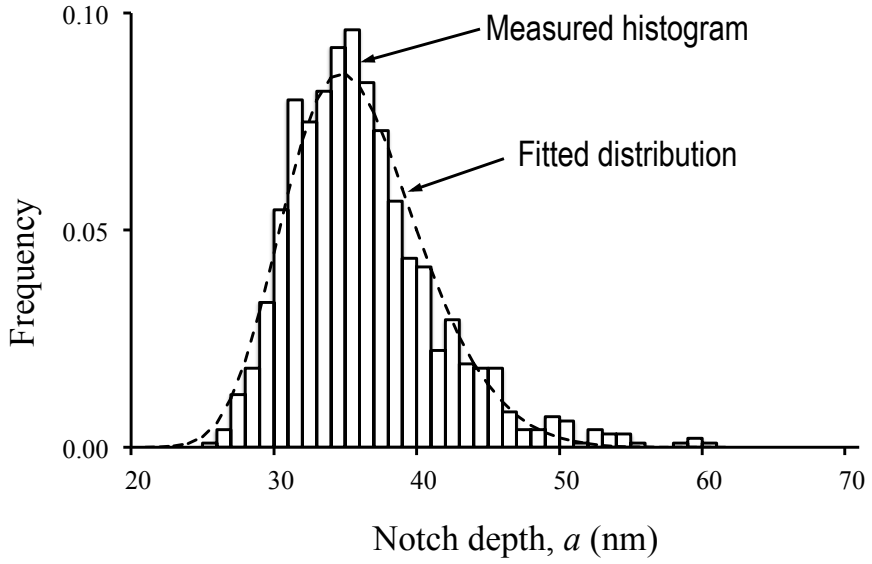

Figure 4.2: Comparison of measured histogram of critical flaw depth and fitted distribution of V-notch depth

The aforementioned bounds of notch angle and depth also ensures that, for any combination of notch angle and depth sampled from the defined distributions, the V-notch can always be contained in a 400 nm long strip of the specimen. In other words, the condition $2a/\cos(\theta/2) < 400$ nm is guaranteed for all possible combinations of a and θ in the distribution.

4.1.2 Stochastic elastic analysis of near-tip stress field

Stochastic analysis is performed to examine the random elastic stress field in a representative element strip of the tensile specimen. According to the assumed probability distribution functions of the notch angle and notch depth, the two geometric parameters were sampled by using the Latin Hypercube Sampling (LHS) technique. As previously mentioned, the poly-Si material is modeled as an isotropic material with a Young Modulus $E = 156$ GPa and a Poisson ratio of $\nu = 0.22$, which are properties shown to be representative of a random aggregate of columnar silicon crystals [5]. The representative element studied was illustrated earlier in Fig.3.2, in which a strip of a poly-Si specimen

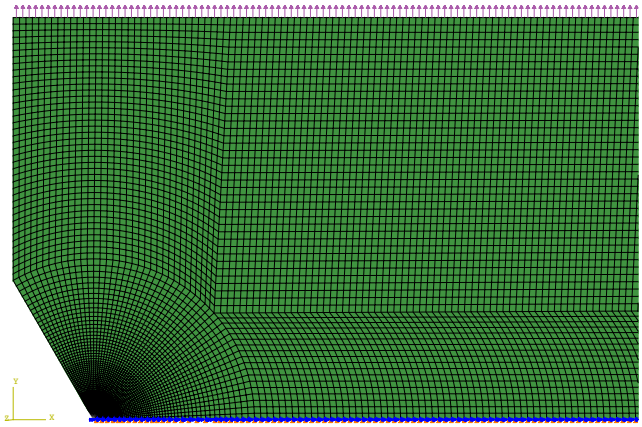

Figure 4.3: Portion of half-element FE model used for computation of near-tip stress field. The full model has width:length ratio of 10:1, so only the left end is shown.

with a width of 2 µm and length of 400 nm contains a V-notch on one sidewall and is subjected to uniaxial tension on the top and bottom surfaces. It can be seen that the geometry of the element is symmetric about its horizontal centerline, and due to the symmetry of the boundary condition, the elastic stress field generated should also be symmetric about the centerline. To obtain tensile stress profile along the notch ligament, finite element (FE) model needs to be created only for half of the representative volume element. A typical FE model and the simulated tensile stress profile along the notch ligament for this realization are shown in Fig.4.3 and Fig.4.4, respectively, for the specific case of $a = 40$ nm, and $\theta = 120$ °. Through a sufficiently large number of realizations (8000), the probability distribution function (pdf) of the dimensionless stress, $f_s(x)$, were obtained numerically, as plotted in Fig. 4.5.

As explained in the previous chapter, the dimensionless stress was calculated for each realization by taking the ratio between the average tensile stress, $\bar{\sigma}$, in the defined 5 nm-wide near-tip region and the farfield stress σ_∞ applied, i.e. $s = \bar{\sigma}/\sigma_\infty$. It must be noted that the computation of $\bar{\sigma}$, with a general form described in Eq.(3.1), cannot be completed merely based on results from the FE model of the sampled specimens, but instead requires a combination of both the numerical computation results and analytical solutions of linear elastic fracture mechanics (LEFM). In the FE model, principal stress σ_{22} were computed for each element in the near-tip region along the notch ligament,

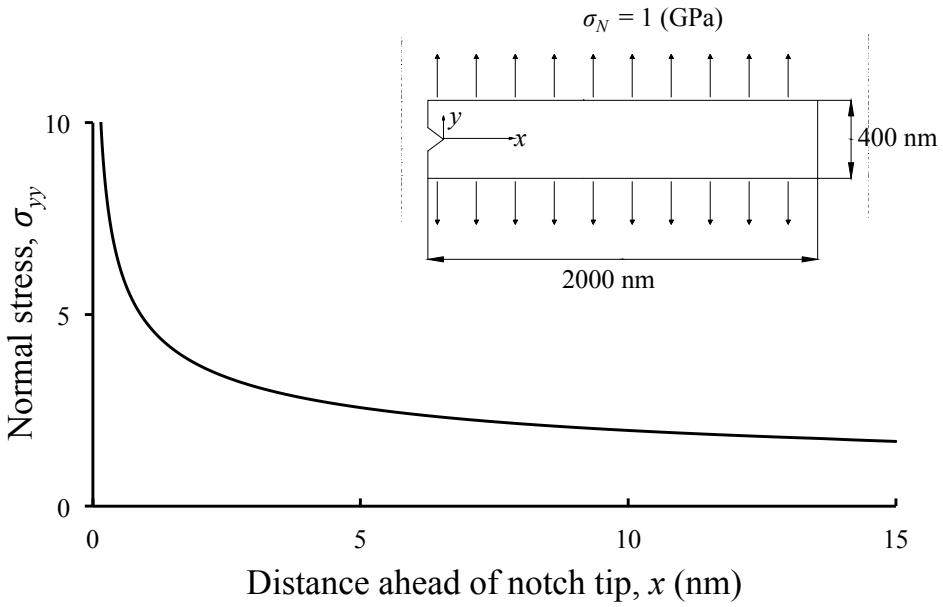

Figure 4.4: Simulated tensile stress profile along notch ligament.

where each value can be interpreted as the size of σ_{22} at the centerpoint of the element. Hence, numerical integration of the principal stresses would give the result:

$$\bar{\sigma}_{Num} \approx \frac{1}{r_c} \int_{r_1}^{r_n} \sigma_{yy}(x) dx \tag{4.3}$$

where r_1 = distance, along the x-direction, between the notch tip and the center of the first element ahead of the notch tip, r_n = distance between the notch tip and the center of the farthest element ahead of the notch tip in the near-tip region, and n = total number of near-tip elements along the notch ligament. Though $r_n = r_c$ is enforced in the descritization process, it is clear that the numerical solution described in Eq.(4.3) does not provide a satisfactory approximation of Eq.(3.1), since the stress between the notch tip and the center of the first element, i.e. $\frac{1}{r_c} \int_0^{r_1} \sigma_{yy}(x) dx$, is not accounted for. Furthermore, LEFM suggests singularity of stress near crack tip, i.e. $\sigma_{yy}(x) \to \infty$ when $x \to 0$, so it would be incorrect to neglect the portion of stress not accounted for in

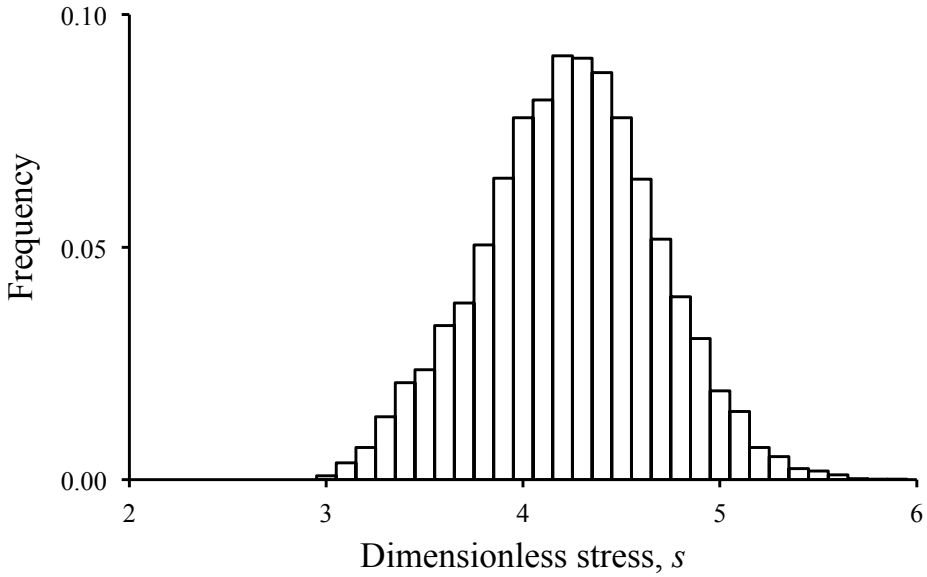

Figure 4.5: Probability distribution of dimensionless stress in V-notch

Eq.(4.3).

According to Williams' solution [**?**], for a V-notch of a given angle θ, σ_{yy} can be approximated as follows:

$$\sigma_{yy}(x) = kx^{\lambda-1} + H.O.T. \tag{4.4}$$

where λ = singularity term corresponding to the notch angle, and $H.O.T.$ = higher order terms that could be approximated as zero when $x \to 0$. For any given angle, λ satisfies the following relation:

$$\lambda \sin(2\alpha) = \pm \sin(2\lambda\alpha) \tag{4.5}$$

where $\alpha = 2\pi - \theta/2$. In the defined distribution of notch angle size, $\theta \in [20°, 140°]$, hence $\theta \in [110°, 170°]$ and $\sin(2\alpha) < 0$. In this case, solution for the singularity term can be simply obtained by finding λ to satisfy $\lambda \sin(2\alpha) = -\sin(2\lambda\alpha)$.

Also note that Eq.(4.4) can be rewritten in a logarithm form as:

$$\ln \sigma_{yy}(x) = \ln k + (\lambda - 1) \ln x + \ln(H.O.T.) \tag{4.6}$$

When x is sufficiently small and the higher order terms are negligible, $\ln \sigma_{yy}(x)$ is linearly related to $\ln x$, with a slope of $(\lambda - 1)$. Based on the FE analysis results, k

Table 4.1: Calibrated statistical parameters of the finite weakest link model

Tensile specimens used for calibration	m	s_0 (GPa)	μ_G (GPa)	δ_G (GPa)	P_{gr}	r_f
$L_g = 20$ nm	64	12.60	19.96	3.50	9.42×10^{-4}	1.0057
$L_g = 70$ nm	65	12.79	19.84	3.40	1.02×10^{-3}	1.0061

can be evaluated for each sampled stress field and $\sigma_{yy}(x)$ can be analytically calculated in the singularity zone. Yet, it must also be noted that the singularity zone does not always extend throughout the defined near-tip region, as the size of the higher-order terms increases following the increase of distance from the notch tip. Though the deviation would be visually unnoticeable on a $\ln x - \ln \sigma_{yy}(x)$ plot, the tensile stress along the notch ligament may become considerably larger than the value predicted by the analytical solution neglecting higher-order terms. Therefore, it is necessary to locate the limit of the singularity zone, $r = r_m$ = distance between notch tip and the center of the m-th element, at which considerably large deviation of $d(\ln \sigma_{22})/d(\ln x)$ from $(\lambda - 1)$ is captured (the deviation tolerance is defined to be 0.5% in this study). Numerical integration will be applied to evaluate average stress in the remaining near-tip region beyond the singularity zone. In summary, $\bar{\sigma}$ is calculated as follows, using trapezoidal method for the numerical integration portion:

$$\bar{\sigma} = \frac{1}{r_c}\left[\frac{k r_m^{\lambda}}{\lambda} + \sum_{i=m}^{n-1} \frac{(r_{i+1} - r_i)(\sigma_{yy,i+1} + \sigma_{yy,i})}{2}\right] \tag{4.7}$$

4.1.3 Calibration of distribution function for random material strength

With the distribution of dimensionless stress obtained for representative material element, the probability distribution functions of material strength, $P_{f_t}(x)$ is calibrated by achieving optimum fits of the measured strength histograms of poly-Si tensile bars. Since strength histograms are available for specimens of two gauge lengths, $P_{f_t}(x)$ is calibrated based on the histogram of one gauge length, and the model is then verified by applying it to predict the strength histogram of the other gauge length. Statistical parameters of $P_{f_t}(x)$, i.e. the parameters in Eqs.(3.3) and (3.4), calibrated based on results of each gauge length is presented in Table 4.1.

It can be seen that the two sets of calibrations yield similar values of the statistical parameters, indicating the relative consistency of the proposed model. The fitted models are presented in Fig.4.6, with comparison to the original experimental data they were each calibrated according to. Furthermore, predictions of strength histogram for specimens of the other gauge length is performed by each model, and compared to the experimental results, as shown in Fig.4.7.

The fact that the present model can reasonably predict the strength distribution of specimens of other gauge lengths confirms its ability to capture the size effect on the probability distribution of poly-Si structural strength. This capability of the model is essential for reliability-based design extrapolation across different specimen sizes. It is also noted that, in both sets of calibrations, the mean strength of each material element, i.e. the Gaussian mean μ_G, is approximately 20 GPa, which is of the order of the theoretical strength of silicon crystals computed by density functional theory. [23]

In the previous chapter introducing the generalized finite weakest link model, it was mentioned that the calibrated values of the parameters in P_{f_t} will depend on the selected size of the near-tip region r_c. In the calibration performed for this study, $r_c = 5$ nm was chosen based on knowledge of the FPZ size in poly-Si. The performance of the calibrated model confirms the general appropriateness of the selected size of r_c, as the model shows a reasonably realistic estimation of the mean strength of poly-Si material element. It must be emphasized, however, that a different value of r_c, would not significantly affect the capability of the calibrated model to capture the size effect on structural strength. Although a different size of r_c will yield a different distribution of dimensionless stress s and effectively alter the values of the parameters in the distribution function of material element strength $P_{f_t}(x)$, the overall functional form of the structural failure probability $P_f(\sigma_N)$ would not be dramatically affected. Given a reasonable selection of r_c, a calibrated model would be expected to display similar effectiveness in predicting the strength histograms of specimens with various gauge lengths, regardless of difference in the $P_{f_t}(x)$ expression.

Table 4.2: Calibrated statistical parameters of the two- and three-parameter Weibull distributions

Tensile specimens used for calibration	m_w	s_w (GPa)	m_1 (GPa)	s_1 (GPa)	σ_0 (GPa)
$L_g = 20$ nm	18.25	3.59	5.78	2.22	1.78
$L_g = 70$ nm	18.45	3.61	3.03	3.66	2.08

4.2 Two-parameter Weibull model

To draw comparison between the present generalized finite weakest link model and the classic Weibull model, fitting of the histogram data will be performed using a two-parameter Weibull distribution. Based on the general form of the Weibull model stated in Eq.(2.5) and also considering that all representative material element in a tensile specimens would share an identical probability distribution of dimensionless stress, the two-parameter Weibull distribution function for the strength of tensile specimens can be rewritten as:

$$P_{w2}(\sigma_N) = 1 - \exp\left[-2n\left(\sigma_N/s_w\right)^{m_w}\right] \tag{4.8}$$

where s_w = Weibull scaling parameter and m_w = Weibull modulus. This can be rewritten as:

$$\ln\left[\ln\left(\frac{1}{1-P_{w2}}\right)\right] = m_w \ln(\sigma_N) + \left[\ln(2n) - m_w \ln(s_w)\right] \tag{4.9}$$

of which $\ln(\sigma_N)$ and $\ln\left[\ln\left(\frac{1}{1-P_{w2}}\right)\right]$ essentially correspond to the horizontal and vertical axes on a Weibull-scale plot of a strength histogram calculated from this model. Hence, by plotting the measured strength histogram on the Weibull scale and fitting the data by a straight line, the corresponding values for m_w and s_w can be easily obtained.

Similar to the aforementioned calibration procedure for the generalized finite weakest link model, the two-parameter Weibull model can be calibrated based on one of the two experimentally obtained strength histograms available, and then predict the other histogram for comparison with the original experimental testing result. Table 4.2 lists the values of m_w and s_w determined by fitting the strength histogram for measurement results for each of the tested gauged lengths.

Variation between the two sets of fitted parameters are insignificant, and thus suggesting that the calibrated values do not strongly depend on which histogram is used for

fitting. However, this does not show that the model effectively captures the size effect on failure probability. It can be clearly seen from Fig.4.8 that the histogram data can not be optimally fitted by a straight line on the Weibull scale, which, as mentioned earlier, has also been the case for many previously obtained strength histogram of MEMS materials. The predicted strength histogram of tensile specimens of each of the two gauge lengths, as predicted by two-parameter Weibull model calibrated from testing results of the other gauge length, is presented in Fig.4.9.

It can be seen that for micrometer-scale poly-Si structures, optimum fitting of the histogram by a linear equation on a Weibull plot only allows for a relatively accurate fitting of what corresponds to the Gaussian core in the generalized finite weakest link model of the material strength. The Weibull tail portion of the histogram obviously deviates from the predicted model — yet the left tail portion of the histogram often contains the low failure probability at which the structure must be designed against.

The deviation of the two-parameter Weibull distribution from the experimental measurement data indicates that this model is inadequate for modeling the failure statistics of poly-Si structures at the length scale concerned. As previously discussed in Chapter 2, the physical reason for the inadequacy of this model is that poly-Si MEMS structures do not contain a sufficiently large number of surface grooves, and therefore have insufficient amount of representative elements for one of the essential assumptions in the Weibull model to be valid. In other words, because Weibull distribution is an asymptotic form describing the extreme value of a large sample, convergence to this function is not expected to be achieved for a small sample.

4.3 Three-parameter Weibull model

As briefly introduced in earlier chapters, the three-parameter Weibull distribution is popularly implemented to provide optimum fit of material strength histogram data. Similar to the two-parameter Weibull model presented earlier, the three-parameter Weibull model initially described in Eq.(2.28) can be simplified as follows for the tensile specimen:

$$P_{w3}(\sigma_N) = 1 - \exp\left[-2n\left(\frac{\langle \sigma_N - \sigma_0 \rangle}{s_1}\right)^{m_1}\right] \tag{4.10}$$

where s_1 = Weibull scaling parameter, m_1 = Weibull modulus, and σ_0 = strength threshold. The parameters m_1, s_1, and σ_0 can be fitted based on either of the provided strength histograms. In specific, the threshold strength value is calibrated first by adjusting σ_0 until the Weibull plot of $\ln(\sigma_N - \sigma_0)$ vs $\ln[\ln(1/(1-P_{w3}))]$ yields an approximately linear relationship. The scaling parameter s_1 and Weibull modulus m_1 can be subsequently determined based on the linear fitting, similar to the calibration procedure of the two-parameter Weibull distribution. The two sets of values for the three parameters calibrated according to the experimentally obtained strength histograms is presented in Table 4.2, and the optimum fitting is shown in Fig.4.10.

Strength histogram for specimens of each of the measured gauge lengths were predicted by model fitted for the other gauge length, and compared to the original data, as shown in Fig.4.11. It can be seen that the calibration result is strongly dependent on the choice of the strength histogram used for fitting. This is further confirmed by the fact that the fitted values for each parameter significantly varies between the two calibrations, as shown in Table 4.2.

It can be observed that prediction of failure statistics using the three-parameter Weibull distribution is strongly dependent on the specific histogram used for calibration, and therefore the functional form does not provide an adequate level of robustness in general. It is also interesting to note that, if the parameters m_1, s_1, and σ_0 were calibrated based on the strength histogram of specimens with 20 µm gauge length, Eq.(4.10) can provide a satisfactory prediction of the strength histogram of the longer 70 µm gauge length specimens. Contrarily, if predictions of the 20 µm gauge length specimen strength were performed using the parameters calibrated according to the strength histogram of the 70 µm gauge length specimens, obvious deviations are present at the left and right tails. By imposing a threshold stress value below which structural failure cannot occur, a calibrated three-parameter Weibull distributions produces a strength histogram with a far-left tail that can only extend to the threshold stress. Histogram testing for specimens with 20 µm gauge length shows cases where failure occurred at a nominal stress below the threshold value for three-parameter Weibull distribution calibrated from the strength histogram of specimens with 70 µm gauge length. Apparently, these data points will deviate drastically from the strength histogram predicted by this model. On the other hand, the model calibrated from the strength histogram of

specimens with 20 µm gauge length has a lower threshold value, and thus will provide a relatively reasonable prediction for failure probability at all applied stress above its defined threshold.

4.4 Discussion

Based on the aforementioned comparison of the present generalized finite weakest link model with the two- and three-parameter Weibull distribution models, it can be concluded that the present model offers a more robust prediction of poly-Si material strength histogram. Although experimental measurement results are available for only two gauge lengths of specimens and the overall size range of the measured specimens is relatively narrow, the obvious flaws of the two- and three-parameter Weibull distributions can still be clearly seen.

To draw further comparisons between the present model and the three-parameter Weibull distribution, models of both types calibrated from the strength histogram of 20 µm gauge length specimens are used to predict structural strength histogram for a wider range of gauge lengths. Fig.4.12 compares the predicted strength distribution for specimens of various gauge lengths, as predicted by the present finite weakest link model and the three-parameter Weibull distribution. It can be seen that for gauge length of 20 µm ($n = 50$), the two models provide reasonably similar predictions of the failure probability, since these models were calibrated based on the measurement of specimens with this gauge length. Nonetheless, apparent deviation between the two models can already be noticed at the tail part of the predicted histograms. At the small size limit, the two model generally displays large difference at the high-probability regime as well as the extreme far left tail. At the large size limit, similar predictions are made for the high-probability regime, while large deviation is observed at the low probability regime. This can essentially be explained by the fact that the two models predict a similar failure probability for representative material element, $P_1(\sigma_N)$, under applied tensile stress approximately within the region $\sigma_N \in [2.0, 3.0]$(GPa). Since for both models, relation between the failure probability of the overall structure and that of the individual element is described by a further simplified version of Eq.(2.1) written as

$$P_f(\sigma_N) = 1 - [1 - P_1(\sigma_N)]^n \tag{4.11}$$

the size of P_f predicted by the two models are expected to consistently match in the region of nominal strengths where the predicted values of P_1 matches, regardless of the gauge length investigated. However, the low probability regime of the small-size structures, where the two models do not match, will dictate a larger region of failure probability for larger-sized structures. As can be seen in Fig.4.12 for the case of $n = 5000$, large deviations between the two models extend approximately to failure probability as high as $P_f = 2.5 \times 10^{-3}$. Once the number of representative elements, n, becomes infinitely large, the entire distribution function of P_f is determined by the far-left tail of P_1. This is exactly why the classic Weibull's model of structural strength is formulated based on an assumption regarding the functional form of the tail of P_1.

The calibrated models can be further compared by using them each to compute design strengths corresponding to demanded reliability. Two typical risk tolerance levels for MEMS structure, 10^{-6} and 10^{-4}, are labeled in Fig.4.12 for each examined gauge length. Interestingly, the generalized finite weakest link model and the three-parameter Weibull distribution provide rather similar predictions of design strengths for most gauge lengths in the typical size range of MEMS components. This is perhaps one of the reasons the three-parameter Weibull distribution is an attractive choice for modeling the failure statistics of MEMS structures. However, this does not completely justify the validity of applying the three-parameter Weibull distribution to predict the strength distribution of a poly-Si MEMS structure. As will be discussed in the next chapter, if the models were extrapolated to different loading configurations, size effect on the failure statistics will vary, and prediction results based on the finite weakest link model and the three-parameter Weibull distribution may deviate more significantly from each other within the typical size range of a MEMS structure.

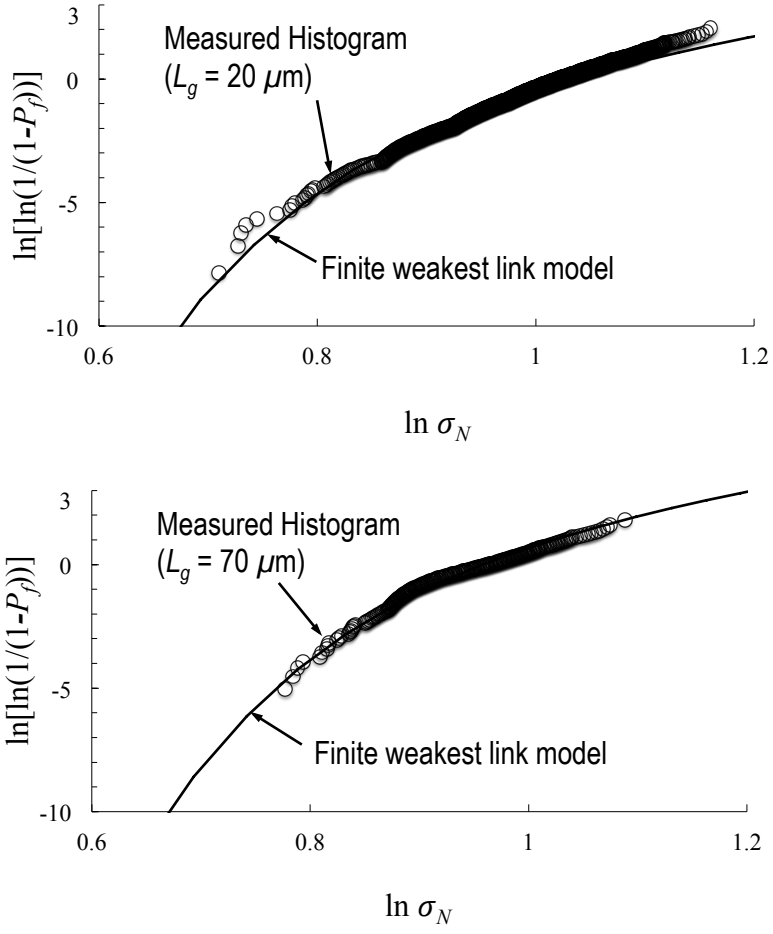

Figure 4.6: Finite weakest link models calibrated for the two sets of experimental results: a) calibrated for strength histogram of 20µm gauge-length specimens; b) calibrated for strength histogram of 70µm gauge-length specimens.

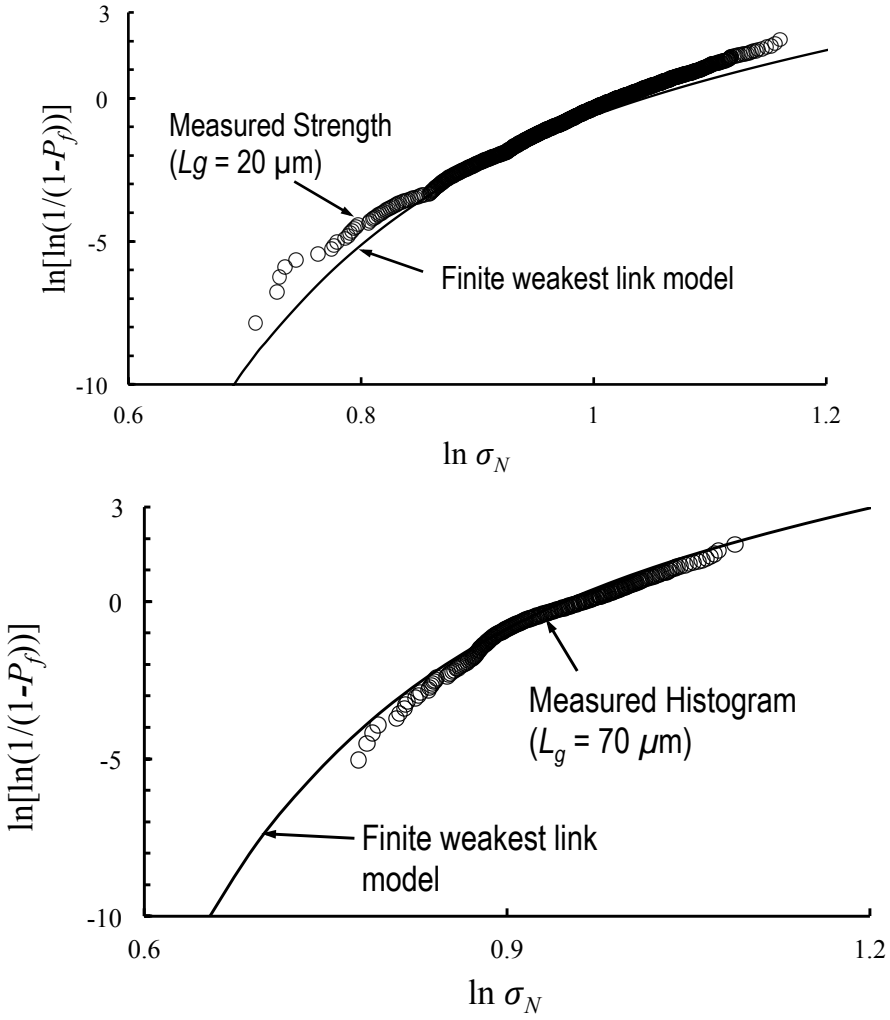

Figure 4.7: Prediciton of strength histograms by finite weakest link model: a) strength histogram of 20μm gauge-length specimens, predicted by model calibrated for 70μm gauge-length specimens; b) strength histogram of 70μm gauge-length specimens, predicted by model calibrated for 20μm gauge-length specimens.

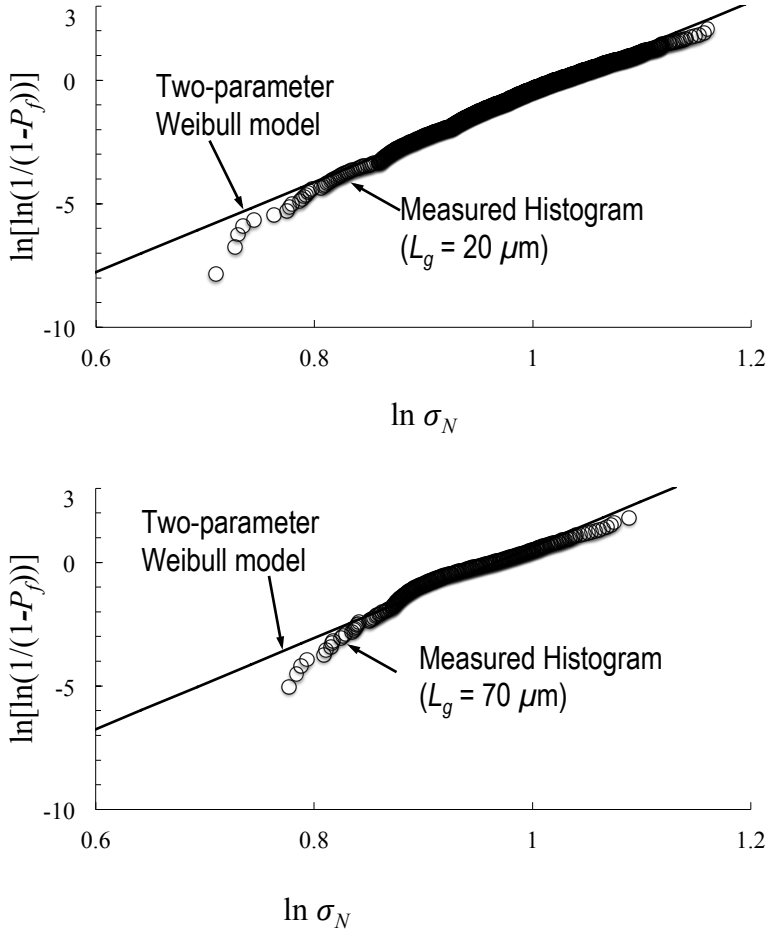

Figure 4.8: Two-parameter Weibull distributions calibrated for the two sets of experimental results: a) calibrated for strength histogram of 20µm gauge-length specimens; b) calibrated for strength histogram of 70µm gauge-length specimens.

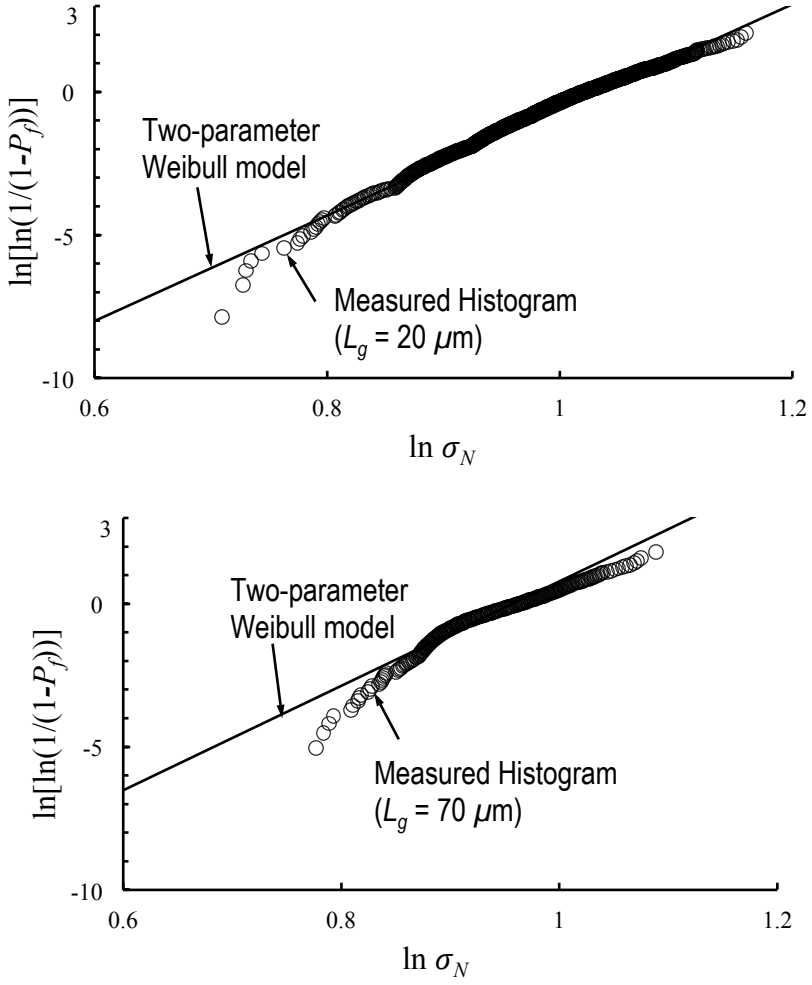

Figure 4.9: Prediciton of strength histograms by two-parameter Weibull distribution: a) strength histogram of 20µm gauge-length specimens, predicted by model calibrated for 70µm gauge-length specimens; b) strength histogram of 70µm gauge-length specimens, predicted by model calibrated for 20µm gauge-length specimens.

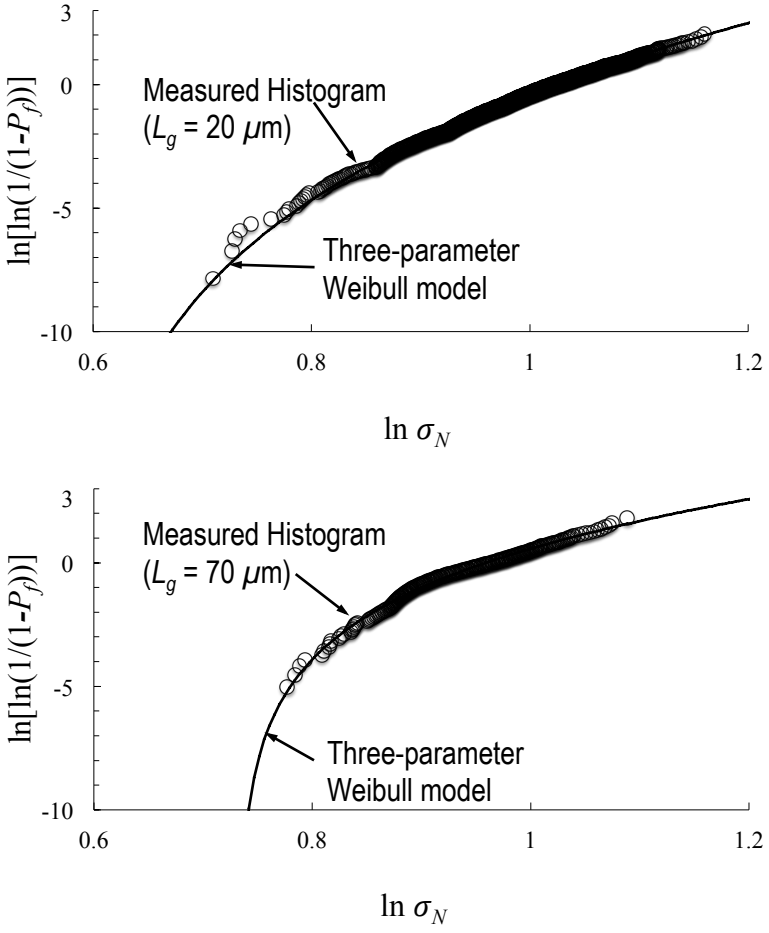

Figure 4.10: Three-parameter Weibull distributions calibrated for the two sets of experimental results: a) calibrated for strength histogram of 20µm gauge-length specimens; b) calibrated for strength histogram of 70µm gauge-length specimens.

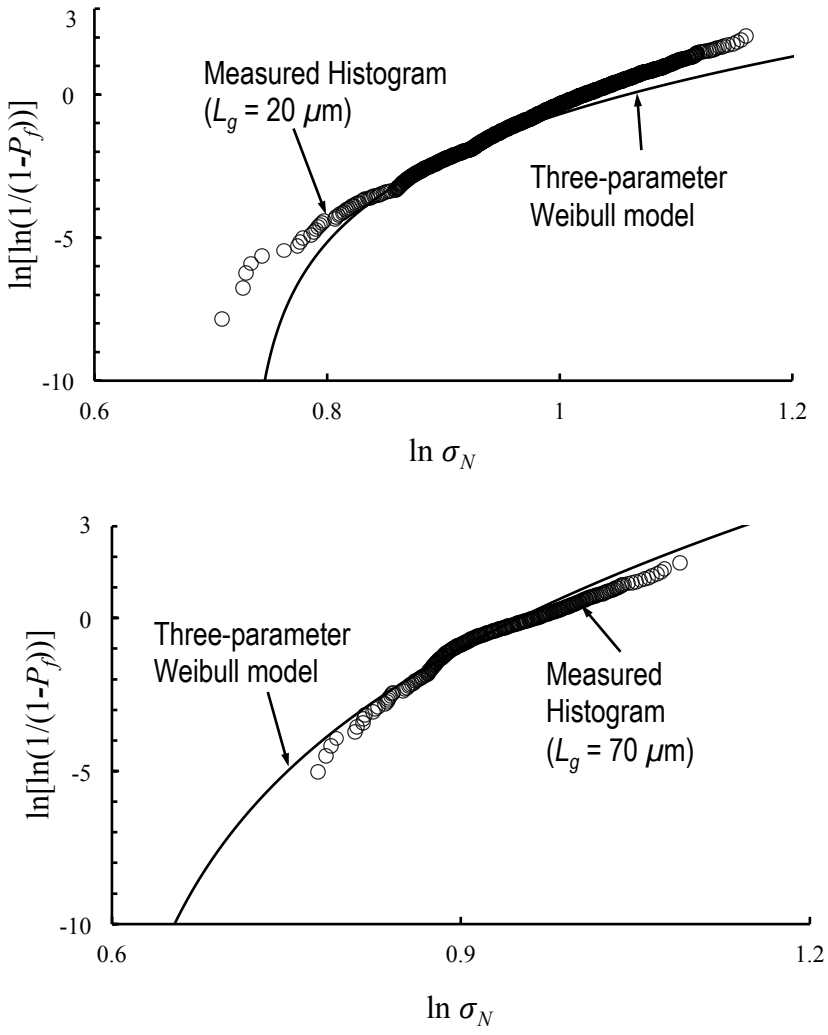

Figure 4.11: Prediciton of strength histograms by three-parameter Weibull distribution: a) strength histogram of 20µm gauge-length specimens, predicted by model calibrated for 70µm gauge-length specimens; b) strength histogram of 70µm gauge-length specimens, predicted by model calibrated for 20µm gauge-length specimens.

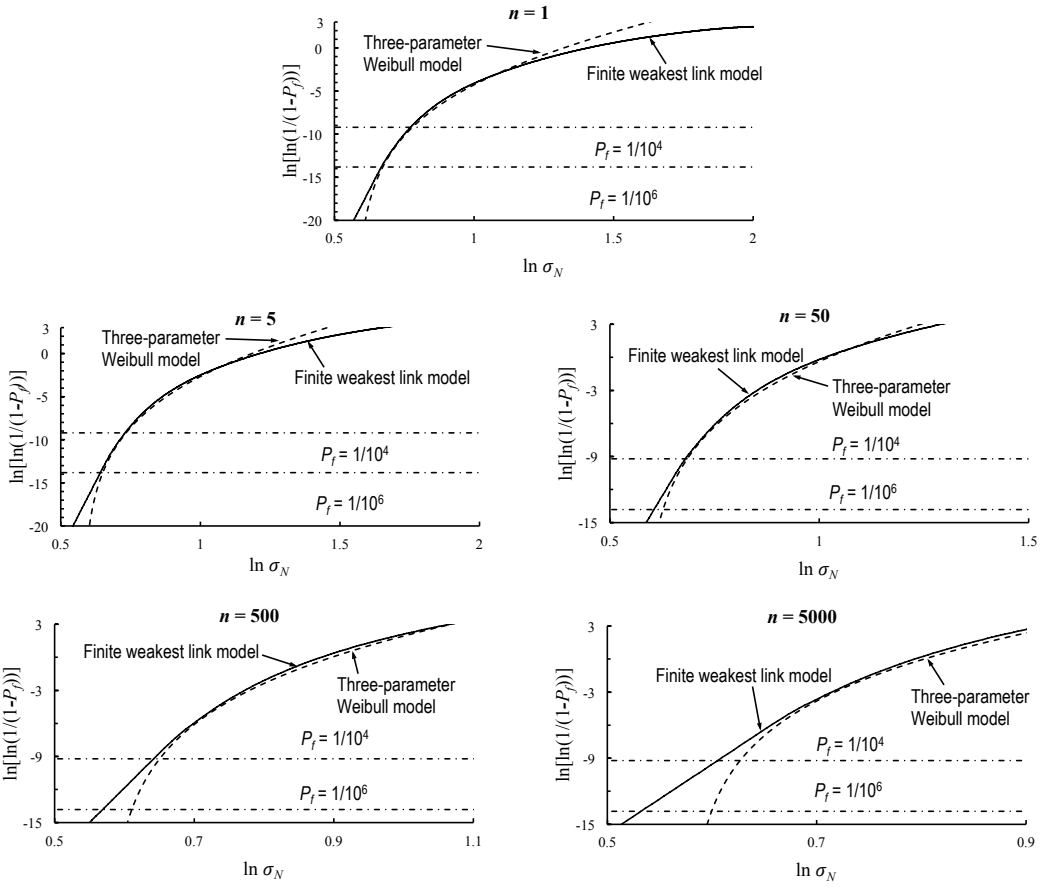

Figure 4.12: Design strengths for poly-Si structure of various gauge lengths under uniaxial tension, corresponding to demanded reliability: a) $n = 1$ ($L_g = 0.4$µm); b) $n = 5$ ($L_g = 2$µm); c) $n = 50$ ($L_g = 20$µm); d) $n = 500$ ($L_g = 200$µm); e) $n = 5000$ ($L_g = 2000$µm).

Chapter 5

Extrapolations for Different Loading Configurations and Mean Size Effect

The previous chapter described the procedure of extrapolating strength statistics of tensile specimens across different gauge lengths. In actual applications of MEMS devices, the structure may be subjected to various loading configurations other than the uniform axial tension case examined earlier. Developing a separate test apparatus for all possible loading configurations is not very feasible, and thus it is critical to perform design extrapolation for specimens based on probabilistic models. As a demonstration, the failure statistics of poly-Si beams subjected to three-point bending will be predicted using the model previously calibrated based on probabilistic failure of tensile specimens.

5.1 Analysis procedure

Consider a poly-Si beam under three-point bending condition, as illustrated in Fig.5.1. The nominal strength of the beam will be defined as: $\sigma_N = 3P_mL/2bD^2$, where P_m = load capacity of the beam, L = beam length, D = beam depth, and b = width of the beam in the transverse direction. For the present computations, consider a set of geometrically similar beams with a constant L/D ratio of 4 and the following different

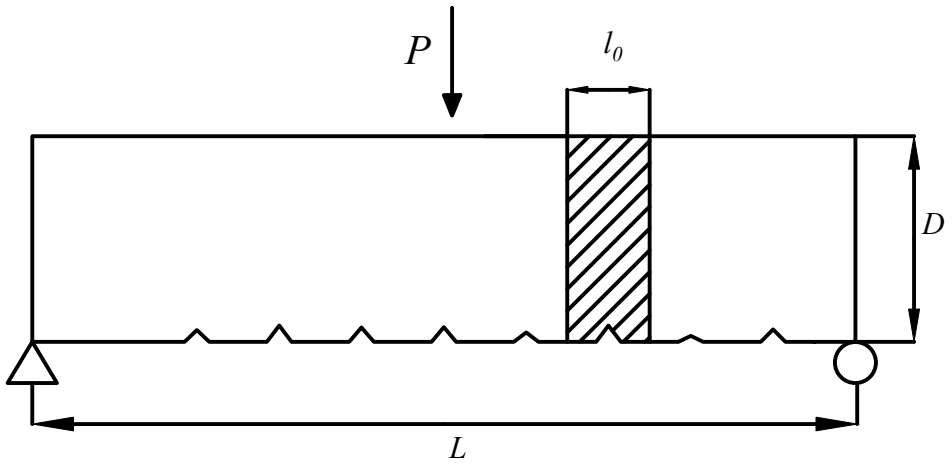

Figure 5.1: Configuration of poly-Si beam under three-point bending condition. Structural failure is initiated by fracture at one of the surface grooves.

lengths: L = 4.8, 10, 20, 40, 80 µm.

It would be reasonable to expect that the failure would initiate from the bottom surface of the beam due to the higher bending stress and stress concentrations at the surface grooves. Similar to the tensile specimens previously analyzed, the location of failure initiation is uncertain, and does not necessarily occur at the point of highest bending stress. Due to the randomness of material tensile strength and surface groove geometry, initial local failure is likely to occur at any of the grooves on the bottom surface of the beam.

As previously mentioned, beams under three-point bending belong to the class of structures of positive geometry. As is the case for the tensile specimens, beams under three-point bending can also be considered to reach its load capacity once a localized crack initiates from one of the surface grooves along the bottom surface of the beam. Hence the overall failure statistics of the beam can be calculated using the weakest link model, where the beam can be considered to consist a number of vertical material strips, each of which contains a V-notch on the bottom surface, as indicated in the shaded region of the beam in Fig.5.1. Assuming a material microstructure similar to

those of the poly-Si tensile specimens, a groove can be expected to also occur at every 400 nm along the bottom surface of the beam, and thus the width of each representative element is set to be l_0 =400 nm.

Yet, different from the previously analyzed tensile specimens, the beam under three-point bending consists of individual material elements subjected to non-uniform bending moments and shear forces. Due to this condition, the relation between the failure probability of a representative element, P_1, and that of the overall structure, P_f, cannot be computed in the simplified form shown in Eq.(4.11), but instead must be calculated according to the generalized form, as previously presented in Eq.(2.1). Therefore, in this study of poly-Si beams under three-point bending, FE simulations will be performed for models of an entire beam, rather than single representative elements each containing a V-notch. To properly calculate the failure probability of the entire beam structure, near-tip stress fields will be computed for all V-notches along the bottom surface of a beam. A general expression for the strength distribution of the entire beam can be expressed as follows:

$$P_f(\sigma_N) = \int_{\tilde{a},\tilde{\theta},\delta} P_f(\sigma_N)|_{\tilde{a},\tilde{\theta},\delta} f(\tilde{a},\tilde{\theta},\delta) d\tilde{a} d\tilde{\theta} d\delta = E\left[P_f(\sigma_N)|_{\tilde{a},\tilde{\theta},\delta}\right] \tag{5.1}$$

where $\tilde{a}$ = random vector containing the values of depth for all V-notches along the bottom surface of the beam, $\tilde{\theta}$ = random vector containing all values of V-notch angle size, δ = random shifting of notch location, $f(\tilde{a},\tilde{\theta},\delta)$ = joint pdf of the random notch depth, angle, and location, $P_f(\sigma_N)|_{\tilde{a},\tilde{\theta},\delta}$ = conditional failure probability of the beam for a given set of values of $\tilde{a}$ and $\tilde{\theta}$, and a value of δ, and $E(x)$ = expectation of x.

The variable δ is introduced here in the study of three-point bending specimens in order to account for the randomness of V-notch location along the bottom surface of the beam. In the previous analysis of tensile specimens, the tip of the ith notch from the top of a tensile bar with gauge length $L = nl_0$ was assumed to be located at $(i - 0.5)l_0$ from the top end of the bar. A similar assumption cannot be made for the bending specimen. Due to the non-uniformity of bending moments and shear forces along the length of the structure, an overall shifting of notch locations will lead to changes in the local stress field near each notch, and therefore the randomness of notch locations must be considered in the stochastic analysis. To incorporate this random factor in the FE realizations, the parameter δ is introduced, and defined to follow a uniform distribution

bounded between 0 and 0.5, with the cdf written as:

$$F_\delta(x) = \frac{x}{0.5} \tag{5.2}$$

For each beam, V-notches is still assumed to be spaced evenly with a distance of $l_0 =$ 400 nm from each other, yet the location of each V-notch along the bottom surface will be shifted rightward by δl_0. In other words, the ith notch from the left of a beam with gauge length $L = nl_0$ is assumed to be located at $(i - 0.5 + \delta)l_0$ from the left end. It is noted that this overall shift of notch location will create a narrow strip at the right end of the beam, possibly with a width insufficient to contain a V-notch. However, the bending moment and shear forces are very small near the ends of a beam, so it is less likely for structural failure to be initiated from a V-notch near the ends of the beam, and thus it can be assumed that the structural failure will not be dictated by surface grooves near the two ends of the beam. Therefore, in the FE simulation, the leftmost and rightmost representative elements in the beam, each with a width of $(1 + \delta)l_0$ and $(1 - \delta)l_0$, respectively, are assumed to not contain V-notches. In each realization, a beam with overall length $L = nl_0$ will thus contain a notch-less element at each end and $(n - 2)$ 400 nm-wide notched element in between, and dimensionless stress field is determined near each V-notch.

It is clear that the conditional failure probability can be calculated using the weakest link model, essentially relating the failure probability at each V-notch to the overall failure probability of the beam structure in the following form:

$$P_f(\sigma_N)|_{\tilde{a},\tilde{\theta},\delta} = 1 - \prod_{i=1}^{n} \left[1 - P_{f_t}\left(\sigma_N s_i|_{\tilde{a},\tilde{\theta},\delta}\right)\right] \tag{5.3}$$

where $n = L/l_0 =$ the number of V-notches along the bottom surface of the beam, $s_i|_{\tilde{a},\tilde{\theta}} =$ dimensionless stress for ith V-notch given its geometric parameters, a_i and θ_i. As defined earlier in Eq.(3.1), the dimensionless stress is the ratio between the average stress in the near-tip region of the specific notch and the nominal stress applied to the structure, i.e. $s_i = \bar{\sigma}/\sigma_N$. In this study, the expectation of $P_f(\sigma_N)|_{\tilde{a},\tilde{\theta}}$ is estimated numerically as:

$$E\left[P_f(\sigma_N)|_{\tilde{a},\tilde{\theta},\delta}\right] = \frac{1}{N_r}\sum_{i=1}^{N_r} P_f(\sigma_N)|_{\tilde{a}_i,\tilde{\theta}_i,\delta} \tag{5.4}$$

where N_r = number of realizations. For each realization, the dimensionless stress field is determined through elastic FE simulations of the beam, of which the notch geometry parameters, angle θ and depth a, are sampled from the defined probability distribution as stated in Eqs.(4.1) and (4.2). An appropriately large value of N_r was determined by conducting convergence test to the computed expectation $E\left[P_f(\sigma_N)|_{\tilde{a},\tilde{\theta},\delta}\right]$, ensuring a relative error below 5%.

5.2 Predictions by Weibull distributions and comparison to present model

As discussed above, the strength distribution of poly-Si beams under three-point bending can be predicted based on a generalized finite weakest link model with statistical parameters calibrated according to the strength histogram of tensile specimens. Similarly, prediction of bending strength can also be performed using the calibrated two- and three-parameter Weibull distributions, and compared to calculation results based on the finite weakest link model.

The general form of two-parameter Weibull distribution for structures of non-uniform stress field is given by Eq.(2.5). Failure is considered to be initiated only along the bottom surface of the beam, which has a linear stress profile for the half-span, i.e.$\sigma_{xx}(x) = 0.5M(x)d/I_{xx} = 3Px/bd^2$, where x = distance from the end of the beam, $M(x)$ = bending moment at x, d = depth of the beam, b = thickness of the beam in the transverse direction, $I_{xx} = bd^3/12$ = moment of inertia, and P = point load applied at mid-span of the beam. By also defining the nominal strength of the beam under three-point bending as $\sigma_N = \sigma_{xx}(L/2) = 3PL/2bd^2$, dimensionless stress will essentially be expressed as $s(x) = 2x/L$, and the constant term, C, in Eq.(2.5) will be rewritten as:

$$C = \frac{1}{l_0}\int_0^L s^{m_w}(x)dx = \frac{2}{l_0}\int_0^{L/2}(2x/L)^{m_w}\,dx = \frac{L}{l_0(m_w+1)} \tag{5.5}$$

Thus the two-parameter Weibull distribution for bending strength of a poly-Si beam will have the following form:

$$P_f(\sigma_N) = 1 - \exp\left[-\frac{L}{l_0(m_w+1)}\left(\frac{\sigma_N}{s_w}\right)^{m_w}\right] \tag{5.6}$$

A similar expression can be derived for the three-parameter Weibull distribution by introducing a strength threshold σ_0. We can first rewrite Eq.(2.4) as:

$$\ln\left[1 - P_f(\sigma_N)\right] = -\int_0^L \left(\frac{\langle \sigma_N s(x) - \sigma_0 \rangle}{s_1}\right)^{m_1} \frac{dx}{l_0} \tag{5.7}$$

Using the expression of the dimensionless stress $s(x)$ as derived for the two-parameter Weibull distribution, the three-parameter Weibull distribution for failure probability under three-point bending can thus be written as:

$$P_f(\sigma_N) = 1 - \exp\left[-\frac{L}{l_0(m_1+1)}\langle 1 - \frac{\sigma_0}{\sigma_N}\rangle^{m_1+1}\left(\frac{\sigma_N}{s_1}\right)^{m_1}\right] \tag{5.8}$$

Note that if we set the strength threshold to be zero, i.e. $\sigma_0 = 0$, the three-parameter Weibull distribution will become the two-parameter Weibull distribution, and Eq.(5.8) clearly matches with Eq.(5.6) since $\langle 1 - \frac{\sigma_0}{\sigma_N}\rangle|_{\sigma_0=0} = 1$.

A comparison of the strength histograms of the geometrically similar set of poly-Si beams as predicted by the generalized finite weakest link model, and the two- and three-parameter Weibull distributions is presented in Fig.5.2. All three models were calibrated based on optimum fitting of strength histogram for the 20 µm gauge length tensile specimens. It can be clearly seen that the predictions by the models differ from each other for beams of all size. This difference appears to be more significant than the difference displayed in the predictions of tensile specimen strength distribution, as shown in Fig.4.12, although a similar range of characteristic sizes were investigated. Due to the non-uniform stress field in the three-point bending configuration, size effect on failure statistics will be different from that of the tensile loading case, and thus specimens of equivalent size will display significantly different nominal strength under different loading configurations.

For example, consider the two-parameter Weibull distribution, which has the simplest functional form. By directly comparing Eqs.(4.8) and (5.6), it can be seen that the strength of a specimen under three-point bending is equivalent to a tensile specimen with a gauge length $2(m_w+1)$ times smaller than that of the beam. With the calibrated value of $m_w = 18.25$, we have the equivalent sizes of a three-point bending specimen and a tensile specimen to differ by a factor of $2(m_w+1) = 38.5$. When subject to equivalent nominal stress loading, a bent poly-Si beam is as strong as a much shorter poly-Si bar under axial tension.

Since a closed-form expression is unavailable for the present finite weakest link model, predicted strength under different loading configurations cannot be analytically compared in a similar manner. Yet, as introduced in Chapter 3, the tail portion of strength distribution must follow a Weibull distribution, and thus an equivalent size relation can still be established for the present model based on the aforementioned case of the two-parameter Weibull distribution. As shown in Tables.4.1 and 4.2, the Weibull modulus calibrated for the two-parameter Weibull distribution and finite weakest link model differ quite significantly, i.e. $m \gg m_1$. For two-parameter Weibull distribution and finite weakest link model calibrated from strength histogram data of tensile specimens with equal gauge length, the equivalent bending specimens will vary significantly in size. This explains the large difference observed in Fig.5.2 for the predicted strength distribution of specimens under three-point bending.

As discussed in the previous chapter, the finite weakest link model and three-parameter Weibull distribution predicted similar design strength corresponding to typical range of risk tolerance level for tensile specimens. However, this is not necessarily the case for specimens subjected to other loading configurations. As the earlier comparison between two-parameter Weibull distribution and the finite weakest link model implies, the change of stress field can lead to a drastic change in the equivalent specimen size. This shows that empirically fitting strength histogram of specimens of one loading configuration or one size does not ensure a robust design extrapolation when the model is applied to other specimens sizes and loading configurations.

To fully validate a probabilistic model for structural strength, it is critical to verify the model with histogram testing of geometrically similar specimens across a sufficiently large range of specimen sizes. As can be concluded based on the foregoing analysis, this verification approach has two main advantages:

1. Provide a more complete model validation against the size dependence of the strength distribution, ensuring reliable design extrapolation across different specimen sizes and geometries;

2. Eliminate the need to measure the far-left tail of the strength distribution, since the tail behavior would be reflected within the bulk part of the strength distribution of large-size specimens.

Certainly, performing histogram testing across a large range of specimen sizes may not be an easily achievable task. In many cases, the size of the test specimens is limited by the test set-up. However, the aforementioned analysis suggests that information regarding the strength distribution of very small or very large specimens can be indirectly obtained by testing specimens of intermediate size under different loading configurations. By taking advantage of equivalent size relations between different stress fields, measurement of a large size range may be effectively achieved with a set of specimens with a small range of sizes. For example, the large-size limit for bending specimens can be analyzed based on uniaxial tension tests, while, on the contrary, the small-size limit for tensile specimens can be achieved through three-point bending tests.

5.3 Mean Size Effect

As indicated in the analysis conducted in Chapter 4, the present finite weakest link model is capable of effectively capturing the size effect on failure statistics of poly-Si structures, and prediction of strength histogram for different gauge lengths matched well with measured results. Additionally, the overall calibration procedure of this model is subjected to a minimal level of ambiguity from a theoretical standpoint.

Earlier overview of the finite weakest link model has shown that the probability distribution of structural strength depends strongly on the specimen size, leading to a size effect on the mean structural strength. This size effect, which was mentioned earlier to differ from the classical Weibull size effect, allows for the determination of the materials strength distribution directly from the size effect curve of the mean strength, in lieu of extensive histogram testings. This indirect method of determining failure probability distribution was proposed by Le and Bažant [24], and has recently been experimentally tested for asphalt mixtures at low temperature, which is also a type of quasibrittle structures whose failure statistics can be explained with the finite weakest link model[25]. This method would require testings at four or five different specimens sizes, with five specimens to determine the mean strength at each specimen size. Alternatively, specimens of same sizes under different loading configurations can also be tested to obtain a similar size effect curve of mean structural strength. The total number of specimens required would thus be significantly lower than what would be needed for a conventional

histogram testing, and would be a much more efficient method for reliability analysis of MEMS devices.

The simple example of tension specimens will be examined here to explain the relationship between mean size effect curve and strength distribution, though a similar relationship can also be formulated for structures of more complex geometries or loading configurations. The overall failure probability of the tensile bar structure is previously expressed in Eq.(3.7). Similar to the determination of nominal strength using the two-parameter Weibull distribution, as stated in Eq.(2.26), the nominal strength can be accordingly calculated based on the finite weakest link model:

$$\bar{\sigma}_N = \int_0^1 \sigma_N dP_f(\sigma_N) = \int_0^\infty \left[1 - \int_0^\infty P_{f_t}(x\sigma_N) f_s(x) dx\right]^{2n} d\sigma_N \tag{5.9}$$

Using the stochastic elastic FE simulation procedure as stated in Chapter 4, the probability distribution of the dimensionless stress, $f_s(x)$, can be calculated based on knowledge of the surface groove geometry and its random distribution. Together with σ_N measured from testing for a sufficiently large range of structure size, i.e. various values of n, the probability distribution of the material element strength $P_{f_t}(x)$ can be determined.

Since $P_{f_t}(x)$ has previously been calibrated for poly-Si tensile bar, the mean size effect curve can be easily produced, and is presented in Fig.5.3. The statistical parameters calibrated according to strength histogram for 20µm-long specimens were used here to predict the mean strength at various gauge lengths. It can be clearly seen that, on the log-log scale, the mean size effect curve deviates from the Weibull size effect, which is expected to strictly follow a straight line on a log-log plot. This is apparently due to the fact that at small sizes, the number of available representative elements in the structure is too low to satisfy the essential criterion for application of two-parameter Weibull distribution. When the structure size increases, the mean size effect curve eventually converges to a straight line with a slope of $1/m$, as shown in Fig.5.3, and thus matches the Weibull size effect.

Due tot the fact that the pdf of dimensionless stress, $f_s(x)$, was computed numerically based on simulations, Eq.(5.9) cannot be analytical integrated to yield a closed-form expression for $\bar{\sigma}_N$. Nonetheless, a general approximation can be achieved by anchoring at the small- and large-size limits, where material strength is assumed to

completely follow a Gaussian and Weibull distribution, respectively. The form of the approximate equation for $\bar{\sigma}_N$ is as follows:

$$\bar{\sigma}_N = \mu_0 \left[\frac{n_1}{n} + \left(\frac{n_2}{n} \right)^{r/q} \right]^{1/r} \tag{5.10}$$

where μ_0 = mean strength of the material element, which can be approximated as the mean of the Gaussian core, μ_G, in Eq.(3.4), and n_1, n_2, r, and q are constants to be calibrated. Further denoting that $C_1 = \mu_0^r n_1$ and $C_2 = \mu_0^q n_2$, a relationship can be established between the aforementioned constants and probability distribution function of material strength P_{f_t}. Eqs.(3.3), (3.4), and (3.5), along with the requirement that $P_{f_t}(\infty) = 1$, together shows that there are four independent parameters in the formulation of P_{f_t}, and thus P_{f_t} can be uniquely defined by the following set of parameters: the Weibull modulus m, the Weibull scaling parameter s_0, the mean of the Gaussian core μ_G, and the standard deviation of the Gaussian core δ_G.

At the large size limit, i.e. $n \to \infty$, the strength distribution of the structure will converge to the Weibull distribution, and P_{f_t} can be approximated as previously shown in Eq.(3.8). Correspondingly, the mean size effect will also converge to the Weibull size effect, and the mean structural strength can be expressed in a manner similar to the general form shown in Eq.(2.27):

$$\bar{\sigma}_N = (2n)^{-1/m} s_0 \Gamma(1 + 1/m) M_m^{-1/m} \tag{5.11}$$

It must also be noted that at the large size limit, Eq.(5.10) can be reduced to $\bar{\sigma}_N \approx \mu_0 (n_2/n)^{1/q}$, which can be equated with Eq.(5.11) to give the following relations:

$$m = q \tag{5.12}$$

$$s_0 = (2M_m)^{-1/m} C_2^{1/q} \Gamma^{-1}(1 + 1/m) \tag{5.13}$$

The above equations, which directly relates the Weibull modulus and scaling parameter to the constants q and C_2, suggests that the Weibull modulus and scaling parameter for the Weibull tail of P_{f_t} can be calculated based on a calibrated expression of the mean size effect curve.

Next, examine the small-size limit, where the material strength is expected to be dictated by the Gaussian core of P_{f_t}. In this case, the structure contains only a single

representative element with a V-notch on each of its two sidewalls. Assuming that the Weibull tail can be neglected at this minimum structural size, the mean structural strength at the small-size limit will have the following approximate form:

$$\bar{\sigma}_N|_{n=1} = \int_0^\infty \left[1 - \int_0^\infty \Phi\left(\frac{x\sigma_N - \mu_G}{\delta_G}\right) f_s(x)dx\right]^2 d\sigma_N \tag{5.14}$$

where $\Phi(x)$ = standard Gaussian distribution of x. According to the above expression, the derivative of $\bar{\sigma}_N$ with respect to n can also be obtained at the small-size limit:

$$\frac{d\bar{\sigma}_N}{dn}|_{n=1} = \int_0^\infty \left[1 - \int_0^\infty \Phi\left(\frac{x\sigma_N - \mu_G}{\delta_G}\right) f_s(x)dx\right]^2 \ln\left[1 - \int_0^\infty \Phi\left(\frac{x\sigma_N - \mu_G}{\delta_G}\right) f_s(x)dx\right] d\sigma_N \tag{5.15}$$

Simultaneously, at the small-size limit, Eq.(5.10) and its derivative with respect to n may be rewritten as:

$$\bar{\sigma}_N|_{n=1} = \left[C_1 + (C_2)^{r/q}\right]^{1/r} \tag{5.16}$$

$$\frac{d\bar{\sigma}_N}{dn}|_{n=1} = -\frac{1}{r}\left[C_1 + (C_2)^{r/q}\right]^{1/r-1}\left[C_1 + \frac{r}{q}(C_2)^{r/q}\right] \tag{5.17}$$

By equating Eq.(5.14) with Eq.(5.16) and Eq.(5.15) with Eq.(5.17), the Gaussian distribution parameters, μ_G and δ_G, can be related to the the constants C_1, C_2, r, and q, and the statistical parameters can be evaluated given a calibrated form of Eq.(5.10).

It can be seen from the foregoing analysis that the statistical parameters controlling the form of P_{f_t} can be evaluated by calibrating an approximate formulation of the mean size effect curve. By evaluating m, s_0, μ_G, and δ_G in this manner, the strength distribution of the material element can be predicted for tensile specimens of any size, as well as poly-Si structures of positive geometry under other loading configurations.

With the statistical parameters for P_{f_t} already evaluated according to strength histogram of tested tensile specimens, the above procedure can be performed in reverse to determine the constants q, r, μ_0, n_1, and n_2. Accordingly, the approximated mean tensile strength at all structure sizes can be calculated to obtain a size effect curve. The approximated size effect curve is plotted in Fig.5.3 along with the mean size effect curve determined based on the failure probability distribution. It can be seen that the approximation agrees well with the size effect calculated from the strength distribution of material element.

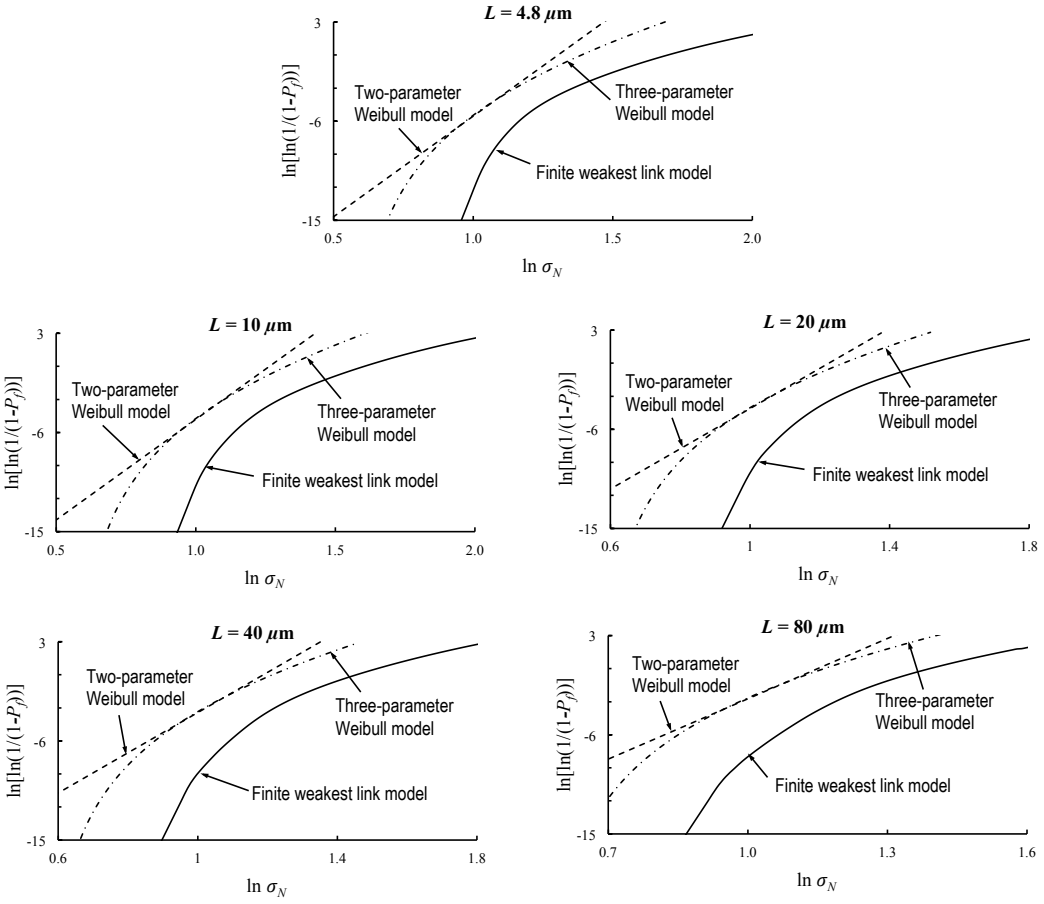

Figure 5.2: Predicted strength histograms for poly-Si beams of various gauge lengths under flexural bending: a) $n = 12$ ($L_g = 4.8$μm); b) $n = 25$ ($L_g = 10$μm); c) $n = 50$ ($L_g = 20$μm); d) $n = 100$ ($L_g = 40$μm); e) $n = 200$ ($L_g = 80$μm).

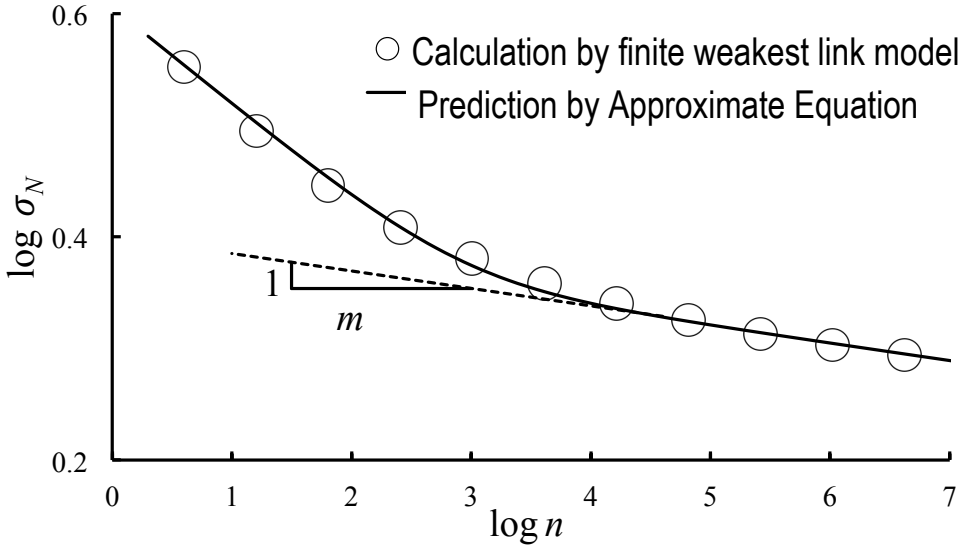

Figure 5.3: Predicted mean size effect curve for poly-Si bars under uniaxial tension.

Chapter 6

Conclusion

This study develops a robust probabilistic model for the strength of poly-Si which can efficiently predict the reliability of MEMS structure of all sizes subjected to various loading configurations.

- The proposed finite weakest link model, which explicitly accounts for randomness of both the material strength and geometrical features of critical flaws in specimens, can effectively describe failure statistics of poly-Si specimens subjected to uniaxial tension. The model can be calibrated by optimally fitting measured tensile strength histograms of poly-Si MEMS specimens of a given gauge length, and provides reliable predictions of failure probability distribution for tensile specimens of other gauge lengths. The choice of the histogram used for fitting is shown to have a minimal effect on the calibration results of statistical parameters in the model.

- The two-parameter Weibull distribution is shown to be incapable of predicting the strength histograms of the two sets of poly-Si specimens measured experimentally. Due to the relatively small number of potential failure locations in the structure, poly-Si MEMS structures cannot satisfy a basic criterion of the Weibull's model to validly predict failure probability of materials. A three-parameter Weibull distribution is shown to improve the quality of optimum fitting. Yet, its prediction capability is limited, as observed from the disparities displayed between statistical parameters calibrated according to two different sets of measured strength

histograms.

- Due to the size dependence of strength statistics, the tail of the probability distribution of strength in small size structure is reflected in the bulk part of the strength distribution for large-size specimens. Rather than performing extensive histogram testings of specimens at a single structure size, the strength distribution of MEMS structures can be experimentally validated by testing a sufficiently large range of specimens sizes. Such a large size range of histogram testing can be achieved not only by altering the physical size of the specimens, but also by adjusting the stress field through change of loading configurations.

- The finite weakest model predicts a strong size effect on the strength distribution, as well as an intricate size effect on the mean structural strength. A direct relationship between the strength distribution and the size effect curve of the mean strength has been shown, and can be utilized to efficiently determine the strength statistics of MEMS structure without conducting histogram testings on a large number of specimens. This alternative method will greatly reduce the cost for experimental procedures required in reliability analysis of MEMS structures.

Bibliography

[1] Alissa M. Fitzgerald, David M. Pierce, Brent M. Huigens, and Carolyn D. White. A general methodology to predict the reliability of single-crystal silicon mems devices. *Microelectromechanical Systems, Journal of*, 18(4):962–970, 2009.

[2] H.D. Espinosa, B. Peng, N. Moldovan, T.A. Friedmann, X. Xiao, D.C. Mancini, O. Auciello, J. Carlisle, and C.A. Zorman. A comparison of mechanical properties of three mems materials-silicon carbide, ultrananocrystalline diamond, and hydrogen-free tetrahedral amorphous carbon (ta-c). In *Proc. 11th Int. Conf. on Fracture (Turin, Italy)*, 2005.

[3] Toshiyuki Tsuchiya, Osamu Tabata, Jiro Sakata, and Yasunori Taga. Specimen size effect on tensile strength of surface-micromachined polycrystalline silicon thin films. *Microelectromechanical Systems, Journal of*, 7(1):106–113, 1998.

[4] Brad L. Boyce, Roberto Ballarini, and Ioannis Chasiotis. An argument for proof testing brittle microsystems in high-reliability applications. *Journal of Micromechanics and Microengineering*, 18(11):117001, 2008.

[5] E David Reedy, Brad L. Boyce, James W. Foulk, Richard V. Field, Maarten P. de Boer, and Siddharth S. Hazra. Predicting fracture in micrometer-scale polycrystalline silicon mems structures. *Microelectromechanical Systems, Journal of*, 20(4):922–932, 2011.

[6] Brad L. Boyce, J. Mark Grazier, Thomas E. Buchheit, and Michael J. Shaw. Strength distributions in polycrystalline silicon mems. *Microelectromechanical Systems, Journal of*, 16(2):179–190, 2007.

[7] Ioannis Chasiotis and Wolfgang G Knauss. The mechanical strength of polysilicon films: Part 2. size effects associated with elliptical and circular perforations. *Journal of the Mechanics and Physics of Solids*, 51(8):1551–1572, 2003.

[8] Kurt E. Petersen. Silicon as a mechanical material. *Proceedings of the IEEE*, 70(5):420–457, 1982.

[9] Roberto Ballarini. Contributive research & development volume 130: The role of mechanics in microelectromechanical systems (mems) technology. Technical report, DTIC Document, 1998.

[10] B.L. Boyce. A sequential tensile method for rapid characterization of extreme-value behavior in microfabricated materials. *Experimental mechanics*, 50(7):993–997, 2010.

[11] Waloddi Weibull. A statistical theory of the strength of metals. *Proc Royal Swedissh Inst. Eng. Research*, (151):1–55, 1939.

[12] Waloddi Weibull. A statistical distribution function of wide applicability. *Journal of applied mechanics*, 1951.

[13] Zdeněk P Bažant and Sze-Dai Pang. Activation energy based extreme value statistics and size effect in brittle and quasibrittle fracture. *Journal of the Mechanics and Physics of Solids*, 55(1):91–131, 2007.

[14] Sze-Dai Pang, Zdeněk P Bažant, and Jia-Liang Le. Statistics of strength of ceramics: finite weakest-link model and necessity of zero threshold. *International journal of fracture*, 154(1-2):131–145, 2008.

[15] Jia-Liang Le, Zdeněk P Bažant, and Martin Z. Bazant. Unified nano-mechanics based probabilistic theory of quasibrittle and brittle structures: I. strength, static crack growth, lifetime and scaling. *Journal of the Mechanics and Physics of Solids*, 59(7):1291–1321, 2011.

[16] Ronald Aylmer Fisher and Leonard Henry Caleb Tippett. Limiting forms of the frequency distribution of the largest or smallest member of a sample. 24(02):180–190, 1928.

[17] Maurice Fréchet. Sur la loi de probabilité de lécart maximum. In *Annales de la societe Polonaise de Mathematique*, volume 6, pages 93–116, 1927.

[18] Horst Rinne. *The Weibull distribution: a handbook*. CRC Press, 2008.

[19] Alfred M. Freudenthal. Statistical approach to brittle fracture. *Fracture*, 2:591–619, 1968.

[20] Zdeněk P Bažant and Sze-Dai Pang. Mechanics-based statistics of failure risk of quasibrittle structures and size effect on safety factors. *Proceedings of the National Academy of Sciences*, 103(25):9434–9439, 2006.

[21] K. Yasutake, M. Iwata, K. Yoshii, M. Umeno, and H. Kawabe. Crack healing and fracture strength of silicon crystals. *Journal of materials science*, 21(6):2185–2192, 1986.

[22] Siddharth S. Hazra, Michael S. Baker, Jack L. Beuth, and Maarten P. de Boer. Demonstration of an in situ on-chip tensile tester. *Journal of Micromechanics and Microengineering*, 19(8):082001, 2009.

[23] S.M.M. Dubois, G.M. Rignanese, Thomas Pardoen, and J.C. Charlier. Ideal strength of silicon: An ab initio study. *Physical Review B*, 74(23):235203, 2006.

[24] Jia-Liang Le and Zdeněk P Bažant. Scaling of static fracture of quasi-brittle structures: Strength, lifetime, and fracture kinetics. *Journal of Applied Mechanics*, 79(3):031006, 2012.

[25] Jia-Liang Le, Augusto Cannone Falchetto, and Mihai O. Marasteanu. Determination of strength distribution of quasibrittle structures from mean size effect analysis. *Mechanics of Materials*, 66:79–87, 2013.